POLITECNICO DI TORINO

Master's Degree in Environmental and Land Engineering

Master's Thesis

Wave attenuation properties of seagrass canopies in combined wave-current flow

Supervisors
Prof. Manes Costantino
Dr. Vettori Davide

Candidate
Giordana Francesco

Academic year 2022/2023

ABSTRACT

In the framework of SHIEELD, a European Research Project with the aim of assessing the protective value of seagrass in nature-based coastal defence, a series of laboratory experiments using artificial vegetation have been performed in an open-channel flume, measuring meadow-induced wave attenuation in combined wave-current flow conditions. Artificial vegetation reproduces four species (*Posidonia oceanica, Zostera marina, Zostera noltii, Cymodocea nodosa)* and four different plant densities; hydraulic conditions imposed allow to replicate a series of current velocities, submergence ratios and wave characteristics observed in the field. Wave attenuation was calculated in terms of the dissipation coefficient $K_{D,wc}$ and compared with dissipation coefficient $K_{D,pw}$ for the corresponding experiment in pure wave conditions, showing general lower dissipation caused by the following current. Two physically-based models present in literature were compared with measured wave dissipation with a decent agreement. The main differences are attributed to uncertainty in the estimation of experimental parameters (drag coefficient C_D and vegetation deflected height h_D), to the wide range of Keulegan-Carpenter numbers KC and vegetation densities involved in experiments and to the different mimic vegetation properties. Further, the dependence of $K_{D,wc}$ on some dimensionless parameters has been investigated, showing that $K_{D,wc}$ increases with plant density and decreases with the Cauchy number Ca and the Keulegan-Carpenter number KC.

TABLE OF CONTENTS

LIST OF FIGURES AND TABLES

Figures

Tables

NOMENCLATURE

A_0	Hydrodynamic forcing in the model of Losada et al. (2016) $[kg/(m^4 s^3)]$
A_w	Wave orbital amplitude at canopy-top $[m]$
a_h	Plant area per unit height normal to the flow $[m]$
a_v	Vegetation frontal area per unit meadow $[1/m]$
a_w	Wave amplitude $[m]$
$a_{w,0}$	Undisturbed wave amplitude $[m]$
B	Buoyancy parameter [–]
B_0	Component related to vegetation-flow interaction in the model of Losada et al. (2016) $[kg/(m^2 s^3)]$
b	Spacing between cylinders in the model of Dalrymple et al. (1984) $[-]$
C	Turbulent stress at canopy top [–]
Ca	Representative Cauchy number [–]
Ca_c	Cauchy number in pure-current conditions [–]
Ca_{pw}	Cauchy number in pure-wave conditions $[-]$
Ca_{wc}	Cauchy number in combined wave-current conditions $[-]$
C_D	Representative drag coefficient for a plant [–]
$C_{D,c}$	Drag coefficient for a plant in pure-current conditions [–]
$C_{D,pw}$	Drag coefficient for a plant in pure-wave conditions $[-]$
$C_{D,wc}$	Drag coefficient for a plant in combined wave-current conditions [–]
$C_{g,pw}$	Group velocity in pure-wave conditions $[m/s]$
$C_{g,wc}$	Group velocity in combined wave-current conditions $[m/s]$
C_M	Inertia coefficient for rigid cylinder [–]
D	Diameter of cylinders in the model of Dalrymple et al. (1984) $[m]$
E	Young modulus $[MPa]$
E_b	Specific energy in respect to the bed $[m]$
E_{wc}	Energy transfer in combined wave-current conditions $[J]$

$F_{D,wc}$	Force acting on the meadow per unit volume volume in combined wave-current conditions $[N]$
g	Gravitational acceleration $[m/s^2]$
H	Wave height $[m]$
H_0	Undisturbed wave height $[m]$
h	Water depth $[m]$
h_D	Vegetation deflected height $[m]$
I	Momentum of inertia $[kg * m^2]$
J	Head drop in respect to bed $[m]$
i	Slope of the bed $[m]$
k	Water depth $[1/m]$
$K_{D,pw}$	Wave dissipation coefficient in pure-wave conditions following the model of Lei & Nepf (2019) $[1/m^2]$
$K_{D,wc}$	Wave dissipation coefficient in combined wave-current conditions following the model of Schaefer & Nepf (2022) $[1/m^2]$
KC	Keulegan-Carpenter number $[-]$
L	Length ratio $[-]$
l	Plant length in still water $[m]$
l_b	Blade length $[m]$
l_e	Generic effective plant length $[m]$
$l_{e,m,c}$	Effective meadow length in pure-current conditions $[m]$
$l_{e,m,pw}$	Effective meadow length in pure-wave conditions $[m]$
$l_{e,m,wc}$	Effective meadow length in combined wave-current conditions $[m]$
l_r	Rigid sheat length $[m]$
n_v	Number of blades per unit area $[-]$
Re_c	Reynolds number in pure-current condition $[-]$
Re_{wc}	Reynolds number in combined wave-current condition $[-]$
S	Average plants spacing $[m]$
Δs	Free surface gradient $[m]$
t_b	Blade thickness $[m]$
U_c	Time-averaged current velocity $[m/s]$

U_w	Orbital wave velocity at canopy-top $[m/s]$
U_1	Total in-canopy current velocity $[m/s]$
$U_{1,c}$	Current-induced in-canopy current velocity $[m/s]$
$U_{1,w}$	Wave-induced in-canopy current velocity $[m/s]$
u_r	Relative velocity between a plant and the combined wave-current field $[m/s]$
u_{wc}	Horizontal flow velocity in combined wave-current conditions $[m/s]$
w_b	Blade width $[m]$
x	Longitudinal coordinate, origin at flume's inlet $[m]$
z	Vertical coordinate, origin at bed level $[m]$
α	In-canopy wave velocity reduction $[-]$
α_D	Wave dissipation coefficient following the model of Dalrymple et al. (1984) $[1/m]$
β_{wc}	Wave dissipation coefficient following the model of Losada et al. (2016) $[1/m]$
δ_E	Distance over which turbulent momentum flux impact canopy velocity $[m]$
ε_D	Energy dissipation per unit horizontal area $[m^2/s^3]$
θ	Vegetation bending angle $[-]$
λ	Wavelength $[m]$
λ_p	Solid volume fraction of the meadow $[-]$
η	Free surface displacement $[m]$
π	Archimedes' constant $[-]$
ρ	Water density $[kg/m^3]$
ρ_b	Density of blade material $[kg/m^3]$
σ	Wave frequency in a wave-current flow $[Hz]$
σ_{wc}	Wave frequency in a reference system moving with current velocity $[Hz]$
υ	Water kinematic viscosity $[m^2/s]$
φ	Plant density $[1/m^2]$

1. INTRODUCTION

Coastal engineering is a branch of civil engineering whose objective is to develop solutions for problems associated with natural and human induced changes in coastal areas that affect human activities (e.g. harbours, recreational beaches). Coastal areas are the margins separating the land from the water and they are composed by sediments derived from land that temporarily forms beaches, bars or islands (USACE, 2002). Because of their nature, coastal areas experience the effect of many physical processes, such as sea level rise, tides and waves, that can induce floods and coastal erosion (the latter is particularly important in non-rocky coasts). They are likely to cause numerous negative impacts, both environmental and economic. Main consequences associated with erosion are degradation of ecosystems, sandy shorelines retreating, loss of productivity of land and infrastructure damage (IPCC AR5, 2014). On the other hand, floods affect freshwater resources, agriculture and forestry, human health, human infrastructures, and biodiversity (IPCC AR5, 2014). Historically, coastal engineering has used hard solutions (also known as grey solutions) to protect shorelines against erosion and prevent floods. This implied the construction of artificial structures such as seawalls, groins, and levees. Over time we have become aware of ecosystems functions and that hard solutions have many consequences. They are very expensive and have a negative impact on aquatic ecosystems, by interfering with natural currents and preventing sediment motion. In light of these considerations, nature-based solutions have been proposed as an alternative and sustainable solution in place of conventional coastal protection. The most diffused nature-based solutions are artificial wetlands or salt marshes, beach nourishment, mangrove re-establishment and protection, oyster reef creation and seagrass/kelp meadows. These ecosystems present a very good adaptation to a variety of conditions, and they can be easily modified in case of need (Davis et al., 2015). Nature-based solutions have been demonstrated to attenuate waves and protect coasts from erosion and floods by stabilizing shorelines and creating low-energy niches in which sediment resuspension is reduced in favour of deposition and retention of

fine material (Schaefer & Nepf, 2022). Moreover, they can help to contrast climate change by increasing the CO_2 storage capacity: submerged aquatic vegetation is an important carbon sink and seagrass meadows can sequester a larger amount of CO_2 per hectare per year than rainforests (Lei & Nepf, 2019b). By contrast, it is very challenging to measure and predict effectiveness of nature-based solutions, leading to high uncertainty about their cost-effectiveness and thus to under-investment (Seddon et al., 2020).

Seagrasses are the largest submerged aquatic vegetation ecosystem protected in Europe (Ondiviela et al., 2014) and provide a potential nature-based solution to reduce wave-generated erosion, as it has been demonstrated that they can affect wave propagation, by reducing wave height and energy by as much as 40% and 50% respectively during storm events (Chen et al., 2022). Besides, seagrasses are ecologically important marine habitat that can stabilize sandy substrates through the effects of their roots and rhizomes (Chen et al., 2022).

1.1. THE SHIEELD PROJECT

In the context of climate change and increased anthropogenic pressure, there is growing literature that physical and environmental pressure on coastal areas are increasing, and this rise is expected to accelerate during 21st century. Sea level rise and more energetic storm patterns associated with climate change will increase exposure rate to coastal flooding and shoreline erosion and will lead to habitat and ecosystem degradation.

SHIEELD is a European Research Project that aims to assess the protective value of seagrass in nature-based coastal defence, and help developing new tools that can be accounted for by stakeholders and policymakers in coastal areas management under a climate change and increased anthropogenic pressure scenario. The project focuses on two main aspects:

- The flow resistance of seagrass canopies in pure-wave flows and combined wave-current flows, with laboratory experiments in an open-channel facility and using seagrass surrogates that mimic the behaviour of real species.
- The effect of seagrass, that shields seabed from wave motion and stabilizes it with rooting system, on sediment transport and sediment mobility threshold, with a dedicated field campaign.

The present work will focus on the first part of the SHIEELD project, namely on wave attenuation properties of mimic seagrass canopies in combined wave-current flows, analyzing the dependence of wave energy dissipation on wave characteristics and meadows properties.

1.2. AIMS AND OBJECTIVES

Main objectives of the present research work are to quantify the wave attenuation (also referred to as wave energy dissipation or wave dissipation in the present work) produced by artificial seagrass in combined wave-current flow conditions, characterize the impact of following currents on wave dissipation, and evaluate if literature's models, based on the assumption of an irrotational and uniform wave-current field, are effective in describing the nonlinear interaction occurring when waves propagate over a current. A series of laboratory experiments have been performed in an open-channel flume with artificial vegetation to achieve these objectives. Mimic vegetation used was designed from dimensionless considerations on morphological and mechanical properties of four seagrass species: *Posidonia oceanica, Zostera marina, Zostera noltii* and *Cymodocea nodosa.* Hydraulic conditions and seagrass shots arrangement were defined for each experiment in order to cover the largest range of field conditions possible observed for the species considered, following similarity considerations. As a result, after a series of preliminary tests, a large number of experiments have been conducted, measuring water depth along the vegetation. Data collected have been processed to estimate wave dissipation and then analyzed in light of the objectives abovementioned.

2. STATE-OF-THE-ART

2.1. WAVE ATTENUATION IN PURE WAVE FLOW

Laboratory, field, and numerical studies concerning the interaction of waves with vegetation mainly deal with the concept of energy dissipation over seagrass, due to reflection and diffraction of wave energy caused by the change in the bottom topography, and with the related wave attenuation.

Research on wave attenuation properties of vegetation canopies has begun in the 80s. Dalrymple et al. (1984) stated that a region of localized energy dissipation attenuates an incident wave field. They proposed a wave dissipation model applicable to monochromatic waves propagating in the x direction through vegetation, over a constant depth:

$$a_w(x) = a_{w,0}\left(\frac{1}{1+\alpha_D x}\right) \tag{2.1}$$

in which α_D is an attenuation factor (wave dissipation coefficient), related to the energy loss and a_w is the wave amplitude (the subscript zero refers to the initial one).

In the framework of the linear wave theory, Dalrymple et al. (1984) obtained wave dissipation coefficient by applying an energy balance and considering a standard quadratic law for energy dissipation. Energy dissipation is due to drag force, exerted by waves on vegetation. Modelling plants as rigid cylinders, they obtained the following formulation for wave dissipation coefficient:

$$\alpha_D = \frac{2C_D}{3\pi}\left(\frac{D}{b}\right)\left(\frac{1}{b}\right)\left(sinh^3(kl) + 3sinh(kl)\right)\left[\frac{4k}{3sinh(kh)(sinh(2kh)+2kh)}\right] \tag{2.2}$$

where C_D is a drag coefficient representative of the flow-plant interaction, D is the cylinder diameter, b is the spacing between cylinders, l is the cylinder height (meaning plant's length in still water), k is the wave number and h is the water depth.
This model, which neglects the effect of plant motion on energy dissipation by including it in the drag coefficient, represents the starting point for any work that has been done so far on the topic of wave energy dissipation by vegetation.

Several studies performed both in laboratory (Stratigaki et al., 2011; Manca et al., 2012) and in the field (Bradley & Houser, 2009; Infantes et al., 2012), confirmed that wave attenuation along artificial vegetation canopies or along seagrass meadows is significant, with wave height decreasing with distance along the canopy. They concluded that wave energy dissipation depends upon several other factors such as vegetation characteristics, weather, hydrodynamic conditions, bathymetry, and sediment characteristics, resulting in a different behaviour for different types of vegetation (Manca et al., 2012). It has been demonstrated that wave attenuation increases with stem density and submergence ratio (Stratigaki et al., 2011; Manca et al., 2012; Luhar et al., 2017). Moreover, it decreases with increasing wave frequency and increases with increasing wave height (Luhar et al., 2017).

The model developed by Dalrymple et al. (1984) works well for rigid vegetation, but flexible seagrass experiences bending and moves with water in a way that the relative velocity u_r between the water and vegetation is not the wave velocity (Luhar et al., 2017; Lei & Nepf, 2019b). Because part of the plants moves passively with waves, vegetation drag and thus wave energy dissipation are lower than for fully rigid blades case with the same geometry (Lei & Nepf, 2019b).
To quantify the impact of blade motion on wave attenuation, Luhar et al. (2017a) proposed the physical concept of effective blade length, defined as the rigid blade length that dissipates the same wave energy as the moving flexible blade. This approach allowed to quantify wave dissipation by considering a rigid vegetation model and thus overcoming the problem of the relative velocity: effect of vegetation

shape and Reynolds number were incorporated into the drag coefficient, in order to estimate C_D from literature, considering non-flexible vegetation, while effects of bending and motion were accounted for through the effective length l_e.

Luhar & Nepf (2016) studied the wave-induced dynamics of flexible blades in a pure-wave flow and determined the coefficient that describes hydrodynamic drag produced by a vegetation stand:

$$C_{D,pw} = \max\left(10KC^{-\frac{1}{3}}, 1.95\right) \tag{2.3}$$

with $KC = U_w T/w_b$, based on Keulegan & Carpenter (1958) and on Graham (1980).
Equation (2.3) assumes that drag is the dominant hydrodynamic forcing and inertial effects are not relevant. The Keulegan Carpenter number KC represents the relative magnitude between drag and inertial forces, thus $KC \gg 1$ is a required condition (Luhar & Nepf, 2016; Luhar et al., 2017).

Luhar & Nepf (2016) also described the deformation of vegetation in response to flow, named as reconfiguration, in terms of wave Cauchy number Ca_{pw}, which is the ratio of the hydrodynamic forcing to the restoring force due to blade stiffness, of blade length ratio L, which is the ratio of the blade length to the wave orbital excursion and of buoyancy parameter B, which is the ratio between the restoring forces due to buoyancy and stiffness.

$$Ca_{pw} = \frac{\rho w_b {U_w}^2 l^3}{EI} \tag{2.4}$$

$$L = \frac{l}{A_w} = \frac{2\pi l}{U_w T} \tag{2.5}$$

$$B = \frac{\Delta \rho g w_b t_b l^3}{EI} \tag{2.6}$$

where $\Delta\rho = \rho - \rho_b$ is the difference in density between water (ρ) and blades (ρ_b), w_b is the blade width, t_b is the blade thickness, U_w is the orbital wave velocity at canopy top, T is the wave period, g is the gravitational acceleration, E the Young modulus and I the moment of inertia.

Based on individual blades analysis, the following scaling laws were proposed to determine the effective plant length l_e, applicable in the wave energy dissipation model, respectively, for large wave excursion ($L \ll 1$) and for small wave excursion ($L \gg 1$), as represented in figure 2.1.

$$\frac{l_e}{l} \sim Ca_{pw}{}^{-\frac{1}{3}} \tag{2.7}$$

$$\frac{l_e}{l} \sim (Ca_{pw}L)^{-\frac{1}{4}} \tag{2.8}$$

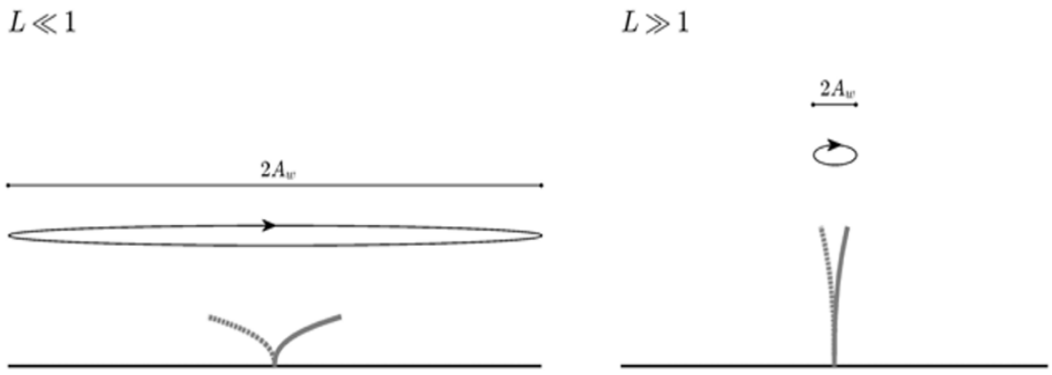

Figure 2.1: schematic illustration of single blade behaviour at large-excursion limit (left panel) and at small-excursion limit (right panel). Figure taken from Luhar & Nepf (2016)

Luhar et al. (2017a) validated equation (2.8) for individual plants within a meadow, while Lei & Nepf (2019b) used the scaling law to construct a predictive model for wave attenuation over a meadow.

They further developed the concept of effective length, by introducing an effective meadow height $l_{e,m,pw}$, that accounts for plant morphology and blade reconfiguration, recognizing that a plant consists of both a rigid (l_r) and a flexible segment (l_b), assumed to behave like an isolated blade of length $l_b = l - l_r$.

$$l_{e,m,wc} = 0.9(Ca_{pw})_b{}^{-\frac{1}{3}} * l_b + l_r \tag{2.9}$$

Moreover, they considered the in-canopy velocity reduction (due to drag exerted by canopy elements) relative to linear wave theory, by introducing the factor α, defined as the ratio of in-canopy to free-stream velocity and computed following (Lowe et al., 2005).

As final result, Lei & Nepf (2019b) proposed the following wave dissipation coefficient:

$$K_{D,pw} = \frac{2}{9\pi} C_{D,pw} a_v k \alpha^3 \left(\frac{9\sinh\left(kl_{e,m,w}\right) + \sinh(3kl_{e,m,w})}{\sinh kh\ (\sinh(2kh) + 2kh)} \right) \tag{2.10}$$

in which a_v is the vegetation frontal area per unit meadow and is calculated as $a_v = n_v w_b$, where n_v is the number of blades per unit area.

$K_{D,pw}$ should be applied in the wave dissipation model based on the formulation proposed by Dalrymple et al. (1984):

$$a_w(x) = \frac{a_{w,0}}{1 + K_{D,pw} a_{w,0} x} \tag{2.11}$$

This model provides a method to predict wave attenuation due to seagrass canopies without requiring a priori measurements of blade posture and produced good predictions for some laboratory and field studies.

2.2. WAVE ATTENUATION IN A COMBINED WAVE-CURRENT FLOW

Wave energy dissipation produced by aquatic vegetation in a combined wave-current flow has been much less characterized compared to the dissipation produced by a pure-wave flow, mainly due to the complexity of the nonlinear interaction between waves and current.

The first studies on the topic gave contradicting conclusions on the effect of a following current on wave dissipation induced by submerged meadows: Li & Yan (2007) presented a numerical model, supported by some laboratory experiments performed with artificial rigid submerged vegetation, that showed a larger wave attenuation in the presence of a combined wave-current flow, compared to the pure-wave case, while Paul et al. (2012) conducted some flume experiments using artificial flexible and rigid submerged vegetation that showed a reduced wave attenuation in the presence of a following current.

Hu et al. (2014) pointed out that the velocity ratio between imposed current velocity and orbital wave velocity at canopy top, i.e. U_c/U_w, was different in the two studies abovementioned. Therefore, they designed a series of experiments in order to investigate the effect of the dimensionless parameter U_c/U_w on wave energy dissipation induced by rigid emerged vegetation in a combined-wave current flow with a following current. Results showed that small current velocities lead to less wave attenuation in comparison to pure-wave conditions, as (Paul et al. (2012), while the opposite, hence larger wave attenuation, happens for higher current velocities, as Li & Yan (2007). Results obtained for rigid submerged vegetation are further corroborated by Yin et al. (2020) and Zhao et al. (2021) and the different behaviour based on U_c/U_w was attributed to changes in wake structure and enhancement of in-canopy velocity.

Two main physically-based models that describe wave attenuation due to aquatic vegetation in a combined wave-current flow are present in literature: Losada et al.

(2016) model and Schaefer & Nepf (2022) model. These models are commented on here and described in their entirety in *Section 2.3.*

Losada et al. (2016) introduced a new analytical model for wave energy dissipation under combined waves and current due to salt marshes based on the energy flux conservation approach presented by Dalrymple et al. (1984) for regular waves and by Mendez & Losada (2004) for random waves. The model was validated by fitting experimental results obtained from tests performed in a large basin at prototype scale using real semi-rigid vegetation species. This formulation is based on the main assumption that the wave-current field is irrotational and uniform, hence their interaction is modelled as linear, in order to obtain an analytical formulation for wave dissipation coefficient. In a range of $0.5 < U_c/U_w < 1.4$, they obtained a smaller wave dissipation when waves and currents are combined, in comparison with pure-wave conditions, in agreement with Paul et al. (2012) and Hu et al. (2014). By fitting experimental results, they obtained an empirical formulation for drag coefficient, incorporating in it the effect of the interaction between meadow density and flow, namely vegetation motion and plant reconfiguration, on wave dissipation along the canopy:

$$C_{D,wc} = 0.25 + \left(\frac{75}{Re_{wc}}\right)^{9} \tag{2.12}$$

where $Re_{wc} = \frac{h_D u_{wc}}{\upsilon}$ is the Reynolds number in combined wave-current conditions, in which the length scale is the deflected height h_D, the velocity scale is the horizontal flow velocity in combined wave-current conditions calculated at canopy top u_{wc} and υ is water kinematic viscosity.

As length scale for the vegetation, they introduced the deflected length h_D, defined as the actual length affecting flow due to bending and based on videorecording of plants bending angle θ during experiments. This parameter does not contain any physical meaning related to plants motion. It only describes the reduction in vegetation frontal area opposed to the flow due to the impact of a following current.

On the other hand, Schaefer & Nepf (2022) proposed a model in which hydrodynamic drag reduction caused by plants motion is considered in the definition of the vegetation effective meadow height, as Lei & Nepf (2019b) did, rather than in the drag coefficient C_D. They obtained the wave energy dissipation coefficient for combined wave-current flows $K_{D,wc}$ in the same form of equation (2.10), with the introduction of a new scaling law as length scale for vegetation in conditions in which both waves and current contribute significantly to hydrodynamic drag and blade reconfiguration ($0.25 < U_c/U_w < 2$):

$$\frac{l_e}{l} = 0.9(Ca_{wc})^{-\frac{1}{3}} \tag{2.13}$$

where the wave-current Cauchy number Ca_{wc} is defined as Lei & Nepf (2019a):

$$Ca_{wc} = \frac{1}{2}\frac{\rho C_{D,wc} w_b {l_b}^3}{EI}\left({U_c}^2 + \frac{1}{2}{U_w}^2\right) \tag{2.14}$$

where $C_{D,wc}$ is the drag coefficient in combined wave-current conditions, U_c is the time-averaged current velocity and U_w is the wave orbital velocity at canopy top calculated from linear wave theory.

Equation (2.13) was demonstrated to predict the effective length reasonably well in wave-dominated ($U_c/U_w < 0.25$) and current-dominated ($U_c/U_w > 2$) regimes as well. Introducing the concept of rigid sheath and flexible blade, as Lei & Nepf (2019b), the vegetation length scale proposed to be applied in equation (2.10) to obtain the wave dissipation coefficient in combined wave-current conditions $K_{D,wc}$ is the following:

$$l_{e,m,wc} = 0.9(Ca_{wc})_b{}^{-\frac{1}{3}} \times l_b + l_r \tag{2.15}$$

Drag coefficient for combined wave-current flows $C_{D,wc}$ has been calculated as in pure wave conditions using equation (2.3), following Sarpkaya & Storm (1985),

that observed a convergence with pure wave values for drag coefficient in combined wave-current flows for $KC > 30$.

In order to validate the use of equation (2.15) in $K_{D,wc}$ formulation, Schaefer & Nepf (2022) performed a series of flume experiments using an artificial seagrass meadow, varying wave characteristics and current velocity. They observed that the ratio between the wave dissipation coefficient in a wave-current and in a pure-wave flow is function of the dimensionless parameter U_c/U_w and of the Cauchy number for pure-wave flow Ca_{pw}.

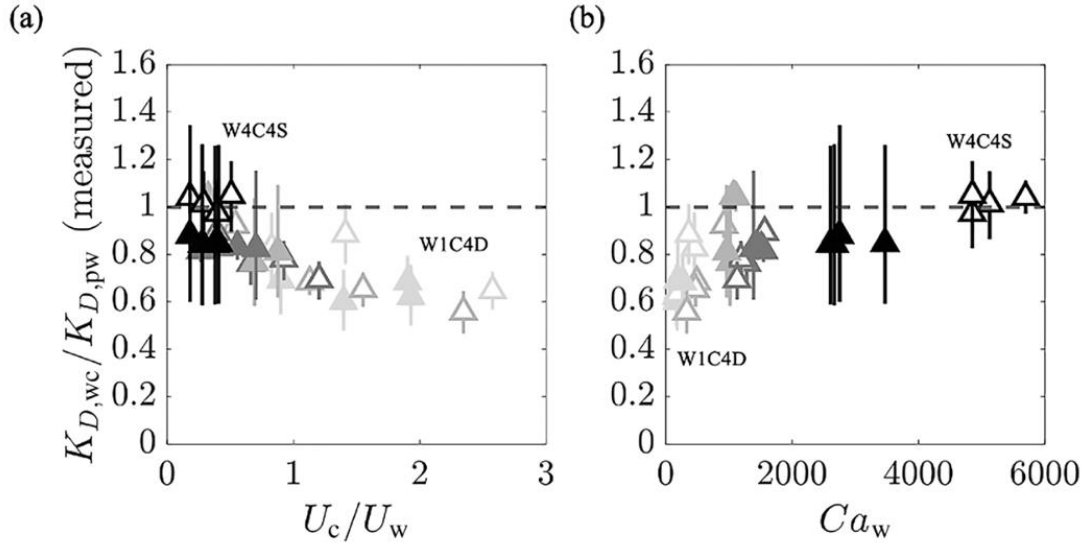

Figure 2.2: measured wave dissipation coefficient $K_{D,wc}$ for wave-current flows normalized by for pure wave conditions $K_{D,pw}$, with the same wave amplitude at the meadow leading edge, as a function of (a) the dimensionless number Uc / Uw and of (b) the wave Cauchy number Ca_{pw}. Figure taken from Schaefer & Nepf (2022)

Specifically, as observed in figure 2.2, the presence of a following current reduced $K_{D,wc}/K_{D,pw}$ when $U_c/U_w > 0.5$, because of the enhanced reconfiguration caused the vegetation current-induced deflection. This is relevant for small wave amplitudes ($Ca_w < 2000$) when wave-induced blade motion is weak, while for high wave amplitudes ($Ca_w > 2000$) the effect of a following current on wave attenuation is negligible due to the strong wave-induced reconfiguration. The reduction of wave dissipation coefficient was observed to reach an asymptote at $K_{D,wc}/K_{D,pw} \approx 0.6$, when $U_c/U_w > 1$.

Schaefer & Nepf (2022) explained the contrast of their results with past literature for rigid meadows (Li & Yan, 2007; Hu et al., 2014) with the current induced reconfiguration of the blades, whose effect of blade-normal relative velocity and vegetation frontal area reduction is greater than the increase in total velocity and thus drag coefficient caused by the current.

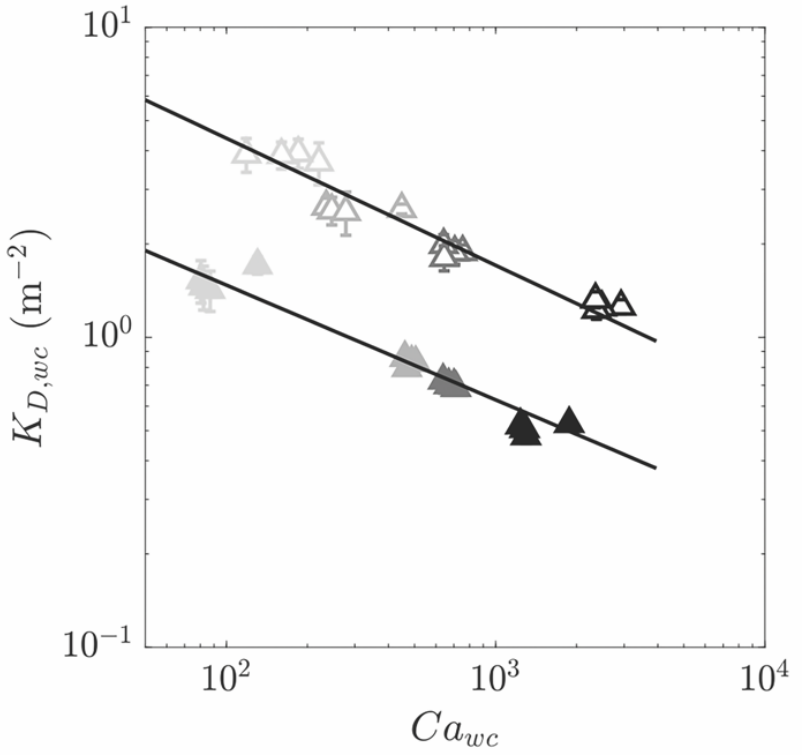

Figure 2.3: Measured wave damping coefficient $K_{D,wc}$ as a function of the wave-current Cauchy number Ca_{wc}. Figure taken from Schaefer and Nepf (2022)

Furthermore, results obtained in terms of $K_{D,wc}$ gave support to the use of the effective meadow length $l_{e,m,wc}$ as predictor of the impact of reconfiguration on meadow drag and wave dissipation. Indeed, the measured power law dependence between $K_{D,wc}$ and Ca_{wc} falls, depending on water depth, between -0.33 and -0.5 (see figure 2.3), which are close to the theoretical dependence derived from their model: $K_{D,wc} \sim {Ca_{wc}}^{-\frac{1}{3}}$ (obtained without considering the dependence of Ca_{wc} on $C_{D,wc}$).

2.3. ANALYTICAL MODELS FOR WAVE ATTENUATION IN A WAVE-CURRENT FIELD

Wave attenuation model by Losada et al. (2016)

The model is based on the following assumptions:

1. Current is uniform over the water depth and alongshore the meadow.
2. Current and waves are collinear.
3. Linear wave theory.
4. Irrotational and uniform wave-current field.
5. Doppler effect is considered in the wave velocity field.
6. Dissipation is only due to drag force.
7. The horizontal drag force component is dominant and drag coefficient is depth-averaged.
8. Constant depth and horizontal bottom.
9. Dense vegetation conditions.

Based on the aforementioned assumptions, the one-dimensional, steady conservation of energy flux equation for waves and current is expressed as:

$$\frac{\partial E_{wc} C_{g,wc}}{\partial x} = -\varepsilon_{D,wc} \tag{2.16}$$

where E_{wc} is the energy transfer in combined wave-current conditions, $C_{g,wc}$ is the group velocity in combined wave-current conditions and $\varepsilon_{D,wc}$ is the energy dissipation per unit horizontal area.

Considering assumptions from (1) to (5), the group velocity $C_{g,wc}$ can be expressed as:

$$C_{g,wc} = \frac{\partial \sigma}{\partial k} = \frac{\partial (U_c k + \sqrt{gk \tanh kh})}{\partial k} = U_c + C_{g,pw}$$
$$= U_c + \frac{1}{2}\left(1 + \frac{2kh}{\sinh (2kh)}\right)\left(\frac{g}{k}\tanh (kh)\right)^{\frac{1}{2}} \qquad (2.17)$$

where the wave frequency σ is equal to $\sigma = U_c k + \sqrt{gk \tanh kh}$, following the dispersion relationship proposed in the linear wave theory by Dean & Dalrymple (1991) for waves propagating over a current with velocity U_c.

Depth-integrated and time-averaged energy transfer in the wave-current field is calculated as Baddour & Song (1990):

$$E_{wc} = \frac{\rho}{16} g \left(1 + \frac{2kh}{\sinh (2kh)}\right)\left(\frac{g}{k}\tanh (kh)\right)^{\frac{1}{2}} H^2$$
$$+ \frac{\rho}{16} g U_c \left(3 + \frac{4kh}{\sinh (2kh)}\right) H^2 \qquad (2.18)$$
$$+ \frac{3\rho}{16} k {U_c}^2 \left(\frac{g}{k}\coth (kh)\right)^{\frac{1}{2}} H^2 + \frac{\rho}{2} h {U_c}^3$$

where H is the wave height.

The first term represents the transport of energy by the wave group velocity; the second term is the transport of energy by the current velocity, considering the work done by current against wave radiation stress; the third and the last term are related to kinetic energy transport performed by current. Summing up, the first term is the wave energy component, the last term the current energy component, while the second and third term represent the contribution of non-linear interaction between current and waves.

Considering assumptions (6) and (7), it is possible to define the depth-integrated (over the canopy height) and time-averaged (over a wave period) energy dissipation per unit horizontal area, considering $z = 0$ at horizontal bottom, as:

$$\varepsilon_{D,wc} = \overline{\int_0^l F_{D,wc} u_{wc}\, dz} = \int_{-h}^{-h+h_D} \frac{1}{2} \rho C_{D,wc} a_h N u_{wc} |u_{wc}| u_{wc}\, dz \tag{2.19}$$

The product $a_h N$ is equal to a_v, the vegetation frontal area per unit meadow volume and $F_{D,wc}$ is the force acting on vegetation per unit volume and according to assumption (6) it is possible to consider only the drag component of this force.
The term u_{wc} is the horizontal flow velocity, and considering assumptions (3), (4) and (5) it can be expressed as:

$$u_{wc} = U_c + \frac{gk}{2(\sigma - U_c k)} H \frac{\cosh(k(h+z))}{\cosh(kh)} \sin(kx - \sigma t) \tag{2.20}$$

Based on assumption (9) of dense vegetation conditions, the oscillatory component can be considered dominant inside the canopy, because currents are diverted around and over the meadow, depending on submergence ratio (Losada et al., 2016), and current contribution in horizontal velocity can be neglected:

$$u_{wc} = \frac{gk}{2(\sigma_{wc})} H \frac{\cosh(k(h+z))}{\cosh(kh)} \sin(kx - \sigma t) \tag{2.21}$$

where $\sigma_{wc} = \sigma - U_c k = U_c k + \sqrt{gk \tanh kh} - U_c k = \sqrt{gk \tanh kh}$ is the wave-current angular frequency introduced by Losada et al. (2016), obtained in a reference system moving with current velocity.

Substituting in equation (2.19), the energy dissipation can be written as:

$$\varepsilon_{D,wc} = \overline{\int_0^{h_D} \frac{1}{2}\rho C_{D,wc} a_v u_{wc}|u_{wc}|u_{wc}\, dz}$$

$$= \int_0^{h_D} \frac{\overline{\frac{1}{2}\rho C_{D,wc} a_v \left(\frac{gk}{2(\sigma_{wc})} H \frac{\cosh\big(k(h+z)\big)}{\cosh(kh)} \sin(kx-\sigma t)\right)^2}}{\left|\frac{gk}{2(\sigma_{wc})} H \frac{\cosh\,(k(h+z))}{\cosh\,(kh)} \text{sin}\,(kx-\sigma t)\right|}\, dz \qquad (2.22)$$

Phase-average of energy dissipation is done by averaging over a wave period $\left(\frac{1}{T}\int_0^T \varepsilon_{D,wc}\, dt\right)$, and then solving the vertical integration. The result is the energy dissipation due to vegetation over a wave period:

$$\varepsilon_{D,wc} = -\frac{2}{3\pi}\rho C_{D,wc} a_v \left(\frac{gk}{2(\sigma_{wc})}\right)^3 \frac{\sinh^3 kh_D + 3\sinh kh_D}{3k\cosh kh} H^3 \qquad (2.23)$$

Substituting equations (2.17), (2.18) and (2.23) in equation (2.16), the energy flux balance becomes a differential equation that can be solved by separating variables and integrating, considering that only the wave height H is function of x. The result is in the form of the wave attenuation model proposed by Dalrymple et al. (1984):

$$H(x) = \frac{H_0}{1+\beta_{wc}x} \qquad (2.24)$$

where

$$\beta_{wc} = H_0 \frac{A_0}{B_0} \qquad (2.25)$$

with

$$A_0 = \frac{2}{3\pi}\rho C_{D,wc} a_v \left(\frac{gk}{2(\sigma_{wc})}\right)^3 \frac{\sinh^3(kh_D) + 3\sinh\,(kh_D)}{3k\cosh^3(kh)} \qquad (2.26)$$

and

$$B_0 = \left[\frac{\rho}{8} g \left(1 + \frac{2kh}{\sinh(2kh)}\right)\left(\frac{g}{k}\tanh(kh)\right)^{\frac{1}{2}} + \frac{\rho}{8} g U_c \left(3 + \frac{4kh}{\sinh(2kh)}\right) + \frac{3\rho}{16} k {U_c}^2 \left(\frac{g}{k}\coth(kh)\right)^{\frac{1}{2}}\right] \times \left[U_c + \frac{1}{2}\left(1 + \frac{2kh}{\sinh(2kh)}\right)\left(\frac{g}{k}\tanh(kh)\right)^{\frac{1}{2}}\right] \quad (2.27)$$

Wave attenuation model by Schaefer & Nepf (2022)

This wave attenuation model is based on the following assumptions:

1. Current is uniform over the water depth and alongshore the meadow.
2. Current and waves are collinear.
3. Linear wave theory
4. Irrotational and uniform wave-current field.
5. Doppler effect is negligible ($C_{g,pw} \gg U_c$).
6. Reduction of the in-canopy wave velocity within the meadow due to canopy drag.
7. Current has an impact on reconfiguration but not significantly increase the total velocity ($U_1 < U_c$).
8. Model valid for rigid vegetation: effect of motion and bending is hidden into the vegetation length scale.
9. Dissipation is only due to drag force.
10. The horizontal drag force component is dominant given the slender morphology of seagrass blades and drag coefficient is depth averaged.
11. Constant depth and horizontal bottom.

Considering assumptions from (1) to (5), the steady wave energy balance is expressed as

$$\frac{\partial E_{wc} C_{g,wc}}{\partial x} = -\varepsilon_{D,wc} \tag{2.28}$$

Based on assumptions (3) and (5) the group velocity for a combined wave-current flow $C_{g,wc}$ can be considered equal to the one for a pure wave flow $C_{g,pw}$, obtained from linear wave theory.

$$C_{g,wc} \approx C_{g,pw} = \frac{1}{2}\left(1 + \frac{2kh}{\sinh(2kh)}\right)\left(\frac{g}{k}\tanh(kh)\right)^{\frac{1}{2}} \tag{2.29}$$

For rigid vegetation, the relative velocity between the vegetation and the water u_r is the absolute fluid velocity u_{wc} within the meadow. Assuming linear wave theory, reduction of in-canopy wave velocity and negligible current velocity impact it is equal to:

$$u_{wc} = a_v \alpha^3 \sigma \frac{\cosh(kz)}{\sinh(kh)} \sin(\sigma t) \tag{2.30}$$

where α is the reduction in orbital velocity due to drag and inertial forces exerted by the canopy elements and is calculated as Lowe et al. (2005)

$$\alpha = \frac{1 - \lambda_p}{1 + (C_M - 1)\lambda_p} \tag{2.31}$$

with C_M inertia coefficient for rigid cylinder and λ_p describing the solid volume fraction.

Depth-integrated and time-averaged energy transfer in the wave-current field is based on Dean & Dalrymple (1991) linear wave theory:

$$E_{wc} = \frac{1}{2}\rho g {a_w}^2 \tag{2.32}$$

Considering vertical blades of a general vegetation length l and assuming (8), (9) and (10) as valid, the rate of energy dissipation by vegetation can be expressed as

$$\varepsilon_{D,wc} = \overline{\int_0^l F_{D,wc} u_{wc}\, dz} = \overline{\int_0^l \frac{1}{2}\rho C_{D,wc} a_v u_r |u_r| u_{wc}\, dz} = \overline{\int_0^l \frac{1}{2}\rho C_{D,wc} a_v |u_{wc}| {u_{wc}}^2\, dz} \tag{2.33}$$

Substituting equation (2.30), solving the vertical integration and phase averaging, equation (2.33) becomes:

$$\varepsilon_{D,wc} = \frac{2}{3\pi}\rho C_{D,wc} a_v \left(\frac{\alpha a_w \sigma}{\sinh(kh)}\right)^3 \left(\frac{9\sinh(kl) + \sinh(3kl)}{\sinh kh\,(\sinh(2kh) + 2kh)}\right) \tag{2.34}$$

Assuming $C_{D,wc}$ and a_v as constant, equations (2.29), (2.32), (2.34) can be substituted in the energy balance (2.28) to yield:

$$\frac{\partial}{\partial x}\left(\frac{1}{2}\rho g {a_w}^2 C_{g,wc}\right) = -\frac{2}{3\pi}\rho C_{D,wc} a_v \left(\frac{\alpha a_w \sigma}{\sinh(kh)}\right)^3 \left(\frac{9\sinh(kl) + \sinh(3kl)}{\sinh kh\,(\sinh(2kh) + 2kh)}\right) \tag{2.35}$$

(2.35) is a differential equation that can be solved by separating variables and integrating, considering that only the wave amplitude a_w is function of x. Result is in the form proposed by Dalrymple et al. (1984):

$$a_w(x) = \frac{a_{w,0}}{1 + K_{D,wc} a_{w,0} x} \tag{2.36}$$

in which the dissipation coefficient in combined wave-current flow $K_{D,wc}$ is defined as:

$$K_{D,wc} = \frac{2}{9\pi} C_D a_v k \alpha^3 \left(\frac{9 \sinh\left(k l_{e,m,wc}\right) + \sinh(3 k l_{e,m,wc})}{\sinh kh \, (\sinh(2kh) + 2kh)} \right) \qquad (2.37)$$

with length scale $l_{e,m,wc}$, defined in equation (2.15) as characteristics vegetation length, which can be better predicted using in the definition of Ca_{wc} (2.14) the total in-canopy current velocity U_1, given by the reduced current velocity $U_{1,c}$ and the wave-induced current $U_{1,w}$, instead of the time-averaged current velocity U_c.
Thus, it follows:

$$Ca_{wc} = \frac{1}{2} \frac{\rho C_{D,wc} w_b {l_b}^3}{EI} \left({U_1}^2 + \frac{1}{2} {U_w}^2 \right) \qquad (2.38)$$

with $U_1 = U_{1,w} + U_{1,c}$, where:

$$U_{1,w} = (0.7 \pm 0.2) * 0.9 \, U_w \sqrt{\frac{a_v k l_{e,m,w}}{\sigma} U_w} \qquad (2.39)$$

$$U_{1,c} = \frac{U_c}{1 - \frac{h_D}{h} \lambda_p \sqrt{\frac{C_{D,c} \, a_v \, l_{e,m,c}}{2C(1-\lambda_p)} \left(\frac{h - h_D}{h} \right)^3}} \qquad (2.40)$$

Here $l_{e,m,w} = 1.1 (Ca_w \mathrm{L})_b^{-\frac{1}{4}} * l_b$ and $l_{e,m,c} = 0.9 (Ca_{wc})_b^{-\frac{1}{3}} * l_b + l_r$ are the effective lengths calculated in wave-dominated $\left(Ca_w = \frac{1}{2} \frac{\rho C_{D,w} w_b {U_w}^2 {l_b}^3}{EI} \right)$ and current-dominated $\left(Ca_c = \frac{1}{2} \frac{\rho C_{D,c} w_b {U_c}^2 {l_b}^3}{EI} \right)$ regimes, λ_p is the canopy solid volume fraction, $C_{D,c} = 195 + \frac{50}{Re_c} = 195 + \frac{50}{U_c w_b / \upsilon}$ is drag coefficient in pure-current conditions and $C = 0.07 \left(\frac{\delta_e}{h} \right)^{1/3}$ characterizes turbulent stresses at the top of the canopy, with $\delta_e = \frac{0.23}{a_v C_{D,c}}$.

3. METHODOLOGY AND METHODS

3.1. EXPERIMENTAL FACILITY

Experiments were conducted in a 50 m long, 61 cm wide and 1 m deep, non-tilting, recirculating, open channel flume located at the Giorgio Bidone Hydraulics Laboratory of Politecnico di Torino (figure 3.1). The flume has glass sidewalls and a bed made mainly of steel and, in some parts, of glass. A false bed of smooth concrete blocks was placed over the original bed of the flume along its entire length, apart from the test section, that starts at $x = 19.751$ m downstream the inlet of the channel. The mimic meadow was mounted above the flume bed in the 4 m test section, by inserting four baseboards with the artificial plants. The x-axis is considered aligned with the length of the flume starting at the inlet, while z-axis is vertical and normal to the bottom of the flume, that is considered as the origin.

Waves were generated by a piston-type wavemaker (figure 3.2) placed in proximity of the flume inlet. It allows to generate waves with a maximum height of 0.3 m and with a wave period between 0.2 and 6 s. Transfer function used to determine actual wave characteristics from imposed oscillatory motion of the wavemaker was known. A 2.2 m long porous steel passive wave-absorber was installed at the end of the flume, just before the outlet, to absorb wave energy and prevent wave reflection to large extents.

Three types of experiments have been performed, involving pure-wave flow, pure-current flow, and combined wave-current flow The outlet of the channel was sealed with a steel cap in pure-wave experiments and with a sharp-crested weir used to regulate water depth in pure-current and wave-current experiments. Current flows in the flume thanks to a submerged pump that enables water recirculation between the flume and a large underground sump, which is connected to the inlet through a pipe were an electromagnetic flow meter was mounted to monitor the flow rate for each test.

Figure 3.1: upstream-downstream view of the large scale open-channel flume at the Giorgio Bidone Hydraulics Laboratory of Politecnico di Torino. Figure taken from Peruzzi (2020)

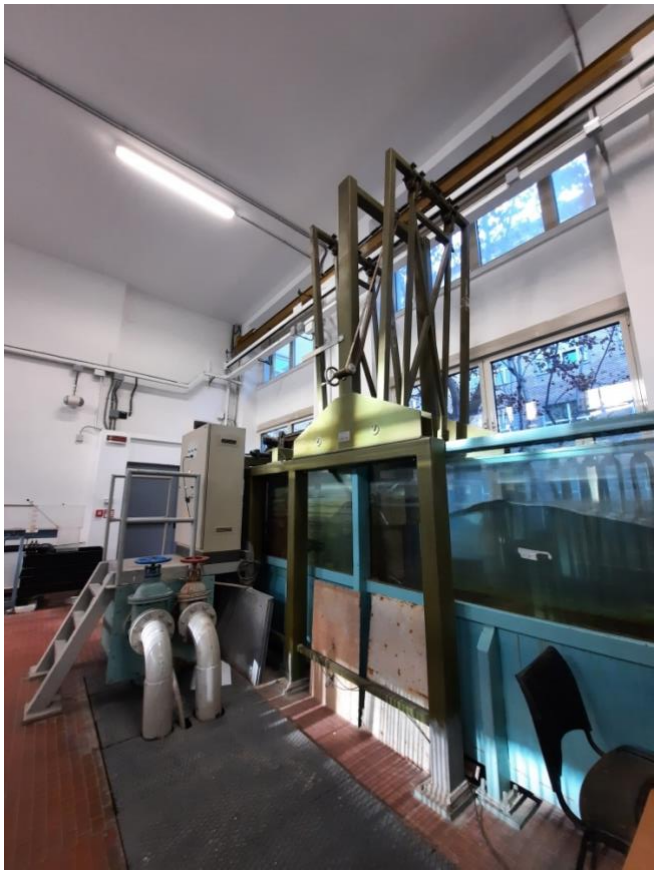

Figure 3.2: view of the piston-type wavemaker at the inlet of the open-channel flume

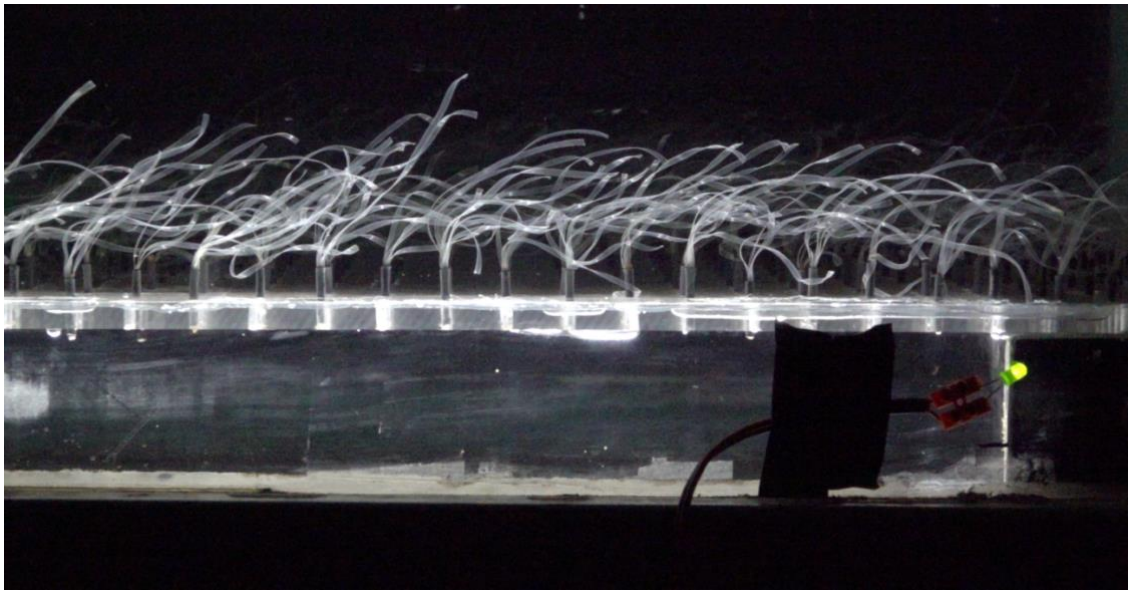

Figure 3.3: view of a detail of the test section with artificial vegetation bended due to the pure-current flow

3.2. INSTRUMENTATION

Wave gauges

Eight wave gauges (WG) connected to a controller were installed on the flume at fixed locations, to measure height of the water column. They operate by measuring the resistance of water between a pair of parallel rods. Resistance is proportional to the immersion depth and is then converted to a length by using an appropriate calibration file. An *Edinburgh Designs WG8USB Wave Gauge Controller* measures the signals from the eight probes and allows the synchronization with the wavemaker for data collection. Probes' sampling rate is 128 Hz and each acquisition lasted for all test duration.

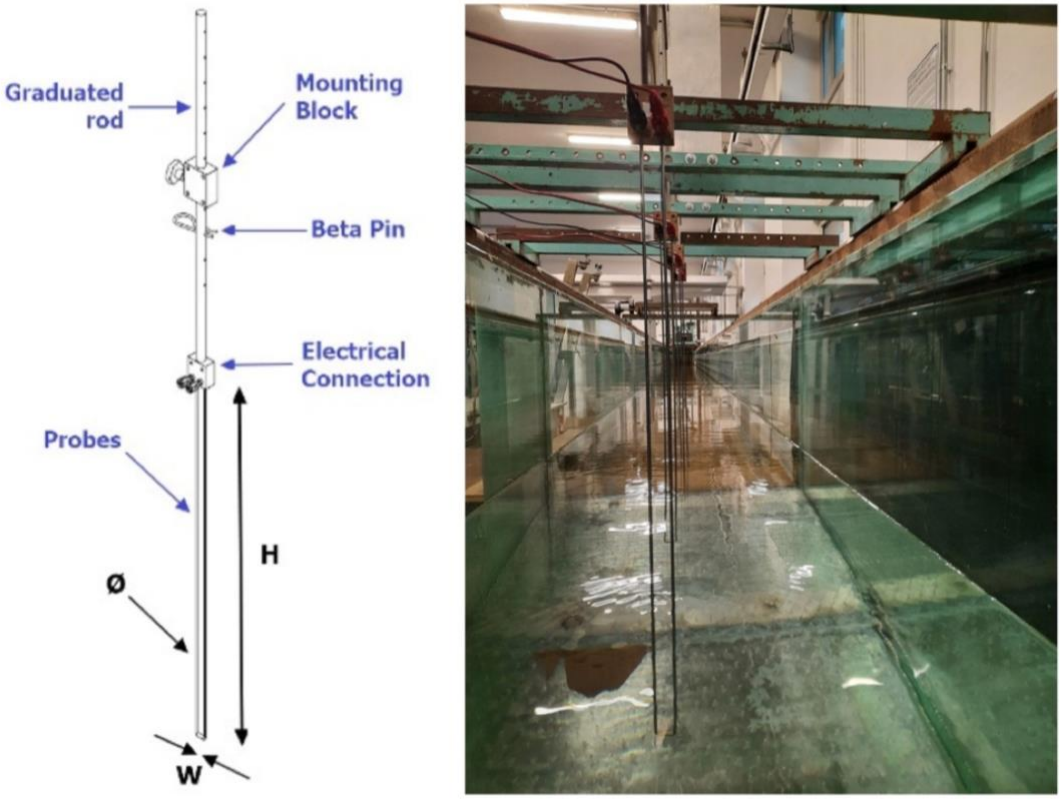

Figure 3.4: scheme of a wave probe (left figure) and probes' installation in the flume (right figure)

Wave gauges were used to measure in eight different locations the water depth at high sampling rate in order to retrieve wave height modifications along the flume. WG1 was placed next to the wavemaker as a reference to control wave generation

mechanism. WG2 was placed just before the meadow and is the reference measurement for wave height attenuation analysis along the canopy $\left(H_0 = H(WG2)\right)$. WG8 was placed immediately after the end of the test section.

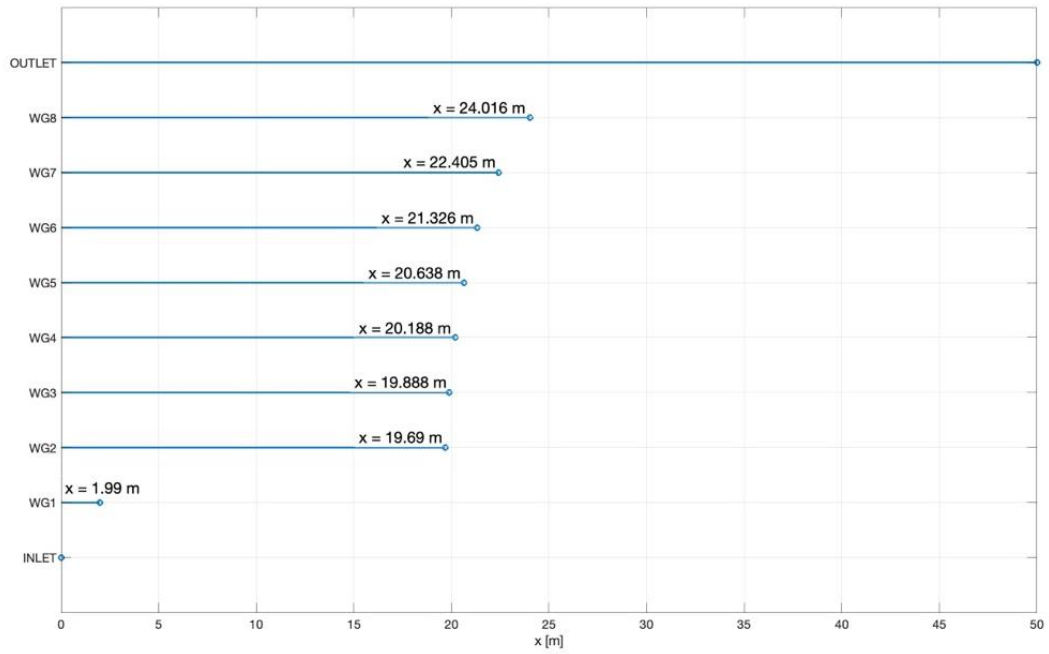

Figure 3.5: scheme of WGs locations along the channel

Electromagnetic flowmeter

An electromagnetic flowmeter *Euromag International MC608 converter* is installed on the main pipe supplying water to the channel and it provides measurements of the flow rate. It works by generateing a local magnetic field and then measuring how the flow modifies it. According to the manufacturer, the accuracy in flow velocity readings is equal to $0.2\% \pm 2$ mm/s.

The flowmeter was used during all the tests to measure the flow rate entering the flume by averaging instantaneous velocities measured in a time interval of 1 minute. Afterwards, values obtained were averaged on the effective test duration in order to calculate, from the discharge rate, the effective current velocity.

Figure 3.6: electromagnetic flow meter

Thermometer

A digital thermometer with a precision of $\pm 0.1°C$ was used to measure water temperature before the realization of each experiment. Measurements were taken immediately downstream the wavemaker. Temperature was recorded in order to assess water viscosity and water density during each test.

Vernier scale

A Vernier scale was installed immediately upstream the test section in order to measure water depth in the flume, mounted on a metal structure which allowed its positioning above the flume. Measurements were used to quantify the exact water depth h at the test section, with a precision of 0.05 mm.

Ultrasonic gauges

Two ultrasonic gauges with a sampling frequency of 100 Hz have been installed before and after the test section, at distance of 6.7 m. They were used to monitor the evolution of free surface in pure-current experiments.

3.3. SEAGRASS MODELLING

Seagrass shoots have been constructed in order to be morphologically and dynamically similar to four seagrass species (*Posidonia oceanica, Zostera marina, Zostera noltii* and *Cymodocea nodosa),* based on field observations and information available in literature.

Each mimic seagrass is composed of 4 low-density polyethylene strips, that mimic plant's leaves, put inside a heat-shrinking sleeve, that mimics plant's rigid sheath (figure 3.7). The number of blades chosen is consistent with field observations for *Zostera noltii, Zostera marina* and *Cymodocea nodosa*, while *Posidonia oceanica* has 7 leaves (de los Santos et al., 2016). The sheath has a diameter of 0.32 cm and is 1 cm long; blades are 9 cm long, 0.2 cm wide and 0.09 mm thick. Hence, total length l of a mimic seagrass in still water is 10 cm. Young modulus E of blade material is 128 MPa and material density ρ_b is 930 kg/m^3. Submergence ratio varies from 0.25 to 0.5 depending on water depth, as explained in *Section 3.4.* In table 3.1 a summary of seagrass biomechanical traits and submergence ratios observed in the field is reported. Data are taken from de los Santos et al. (2016), Vettori & Marjoribanks (2021), Soissons et al. (2018) and Schaefer & Nepf (2022).

Table 3.1: seagrass properties observed in the field

	thickness [mm]	width [mm]	length [m]	Young modulus [MPa]	Submergence ratio [−]
Cymodocea nodosa	$0.1 - 0.4$	$2.6 - 4.7$	$0.1 - 0.55$	$55 - 105$	$0.1 - 1$
Posidonia oceanica	$0.2 - 0.5$	$9 - 10.8$	$0.15 - 0.75$	$110 - 470$	$0.02 - 0.5$
Zostera marina	$0.15 - 0.44$	$3 - 12$	$0.15 - 0.8$	$100 - 380$	$0.1 - 0.5$
Zostera noltii	$0.16 - 0.26$	$2 - 2.7$	$0.05 - 0.27$	$75 - 1000$	$0.1 - 1$

Figure 3.7: shoots of mimic seagrass used in the experiments

Mimic plants were inserted in four predrilled boards made in plexiglass, each board is 1 m long and 0.61 m wide, for a total meadow length of 4 m and a total meadow area of 2.44 m^2. Then, baseboards have been placed into the flume at the test section, creating the meadow.

Four different meadow densities were used in the experiments: 251, 502, 669 and 1338 $plants/m^2$. In the next paragraphs, they will be indicated respectively as Veg251, Veg502, Veg669 and Veg1338. In figure 3.8 it is shown the stem configuration for meadow density 669 $plants/m^2$. Densities were selected based on seagrass data present in the literature:

- Ondiviela et al. (2014) reported a density from 600 to $4000\ \mathrm{plants/m^2}$ for *Zostera noltii* in the field;
- Schaefer & Nepf (2022) reported a density from 350 to $2200\ \mathrm{plants/m^2}$ for *Zostera marina* in the field;
- Infantes et al. (2012) reported a $2200\ \mathrm{plants/m^2}$ density for *Posidonia oceanica* in the field.

Belcher et al. (2003) predicted that dense canopy regimes occur for:

$$\frac{t_b}{S^2} l > 0.1 \tag{3.1}$$

where S is the average plant spacing.

Considering that in densest condition tested (Veg1338) $S^2 \sim 7.4\ \mathrm{cm}$, it follows $\frac{t_b}{S^2} l < 0.1$ for every stem density used in the present study, and thus all tests are performed in condition of non-dense canopy.

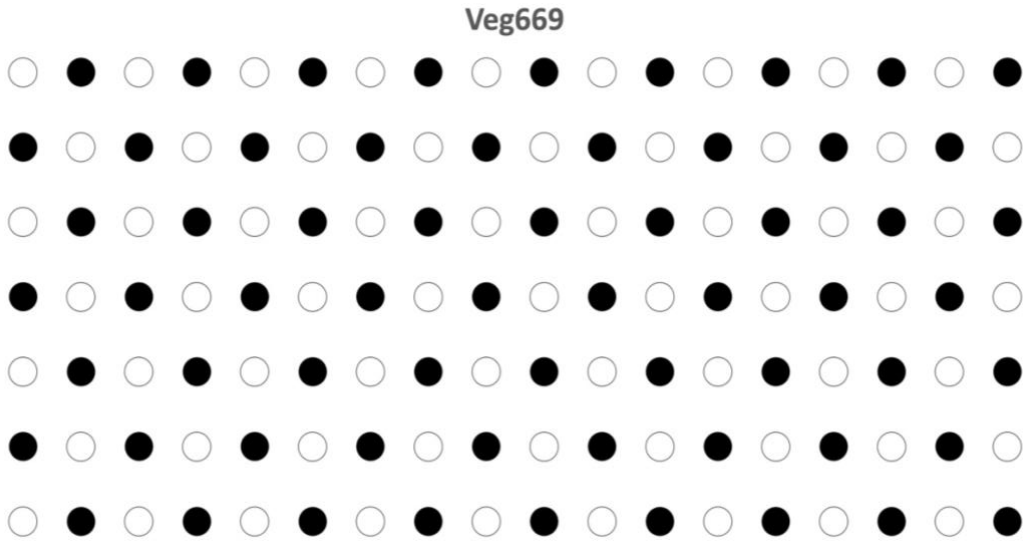

Figure 3.8: detail of shoots arrangement for Veg669. Filled circles are holes in which is placed a plant; empty circles represent empty holes.

3.4. EXPERIMENTAL DESIGN

Experiments were designed following similarity considerations in order to make them representative of field conditions. Froude number Fr, Cauchy number Ca, buoyancy parameter B and length ratio L were used to assess scaling ratio for length r_l and, referred to it, for velocity $\left(r_u = \sqrt{r_l}\right)$, Young modulus $(r_E = r_l)$ and time $\left(r_t = \sqrt{r_l}\right)$. Scaling ratios achievable in terms of length to reproduce the four seagrass species vary from 1 to 8. The effect of turbulence is considered negligible and the Reynolds number Re was not used in the similarity considerations.

Three experimental water depths were used: $20, 30$ and 40 cm, and that allowed to reproduce water depths from 20 cm to 3.2 m in the field. They will be indicated respectively as h20, h30 and h40 in the next paragraphs. The corresponding submergence ratios l/h, hence the fraction of water depth occupied by plant height, were respectively: $0.50, 0.33$ and 0.25, in accordance with field data reported in table 3.1. Wave heights were selected to cover all the wavemaker operative range, in accordance with its limitations related to water depth, which varies between 0.01 m and 0.15 m, means wave heights from 0.01 m to 1.2 m in the field. Wave periods were designed to vary between 0.81 s and 2.20 s, corresponding to a range from 0.81 s to 6.22 s in the field.

Current velocities were designed in order to be representative of field conditions and to cover the widest possible range of U_c/U_w. Folkard (2005) reported a velocity range of $0.08 - 0.4$ m/s for *Posidonia oceanica* and Schaefer & Nepf (2022) of $0.01 - 0.55$ m/s for *Zostera marina.* Three depth-averaged current U1, U2 and U3 have been used and they correspond respectively to 0.075, 0.125 and 0.175 m/s, which represent velocities from 0.075 m/s to 0.49 m/s in the field, and that make vary U_c/U_w between 0 and 12. For a relevant number of tests, it was imposed $U_c/U_w < 0.5$, that is the transition value indicated by Schaefer & Nepf (2022) above which the reduction in wave attenuation due to presence of the current is relevant. Moreover, some tests were designed with $U_c/U_w > 3$ in order to broaden the range studied by Schaefer & Nepf (2022).

Combining all the values for the parameters described above, a set of 27 experiments have been performed for each current velocity and thus a set of 81 experiments have been performed for each of the four vegetation densities involved, plus for the condition of unvegetated bed, resulting in 405 experiments overall. A summary of the hydraulic and wave conditions for each set of experiments is shown in table 3.2. Based on the wave characteristics reported in table 3.2, the Le Méhauté's diagram of wave theories validity (Le Méhauté, 1969) was used to assess the most appropriate wave theory to describe waves employed in the experiments (see figure 3.9)

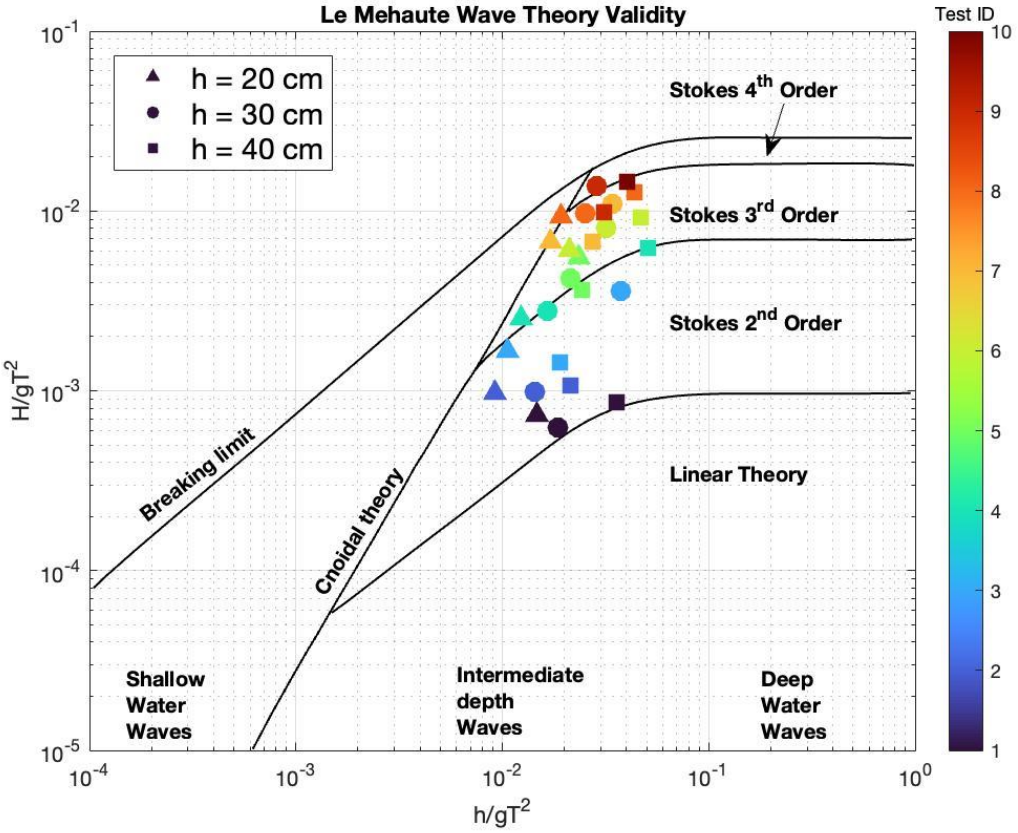

Figure 3.9: Le Méhauté's diagram of wave theories validity.

All the waves employed fall outside the region of validity of the linear wave theory. They mainly belong to the Stokes' 2nd order and Stokes 3rd order regions. The higher is the wave height, the more waves are nonlinear. However, as will be explained in the next chapter, waves will be analyzed considering linear theory so that to

compare results with the models from the literature in which the interaction between waves and current has been modelled as linear. Therefore, any mismatch between the results and the models could be due (at least partially) to nonlinear interactions between waves and current. Further, all the tested waves fall in the range of intermediate depth, defined as $\pi/10 < kh < \pi$ (Dean & Dalrymple, 1991).

Table 3.2: summary of wave and hydraulic conditions for experiments performed for each current

h [m]	TEST	T [s]	H [m]	L [m]	KC	U_C / U_W for U_c=0.075 m/s	U_C / U_W for U_c=0.125 m/s	U_C / U_W for U_c=0.175 m/s
0.2	ID01	1.38	0.010	1.8	22	2.4	3.9	5.5
0.2	ID02	2.20	0.021	3	78.6	1.1	1.8	2.5
0.2	ID03	1.93	0.031	2.6	100.7	0.7	1.2	1.7
0.2	ID04	1.65	0.041	2.2	11.1	0.6	0.9	1.3
0.2	ID05	0.87	0.047	1	55	0.6	1.0	1.4
0.2	ID06	0.96	0.057	1.15	77.8	0.5	0.8	1.1
0.2	ID07	1.18	0.078	1.5	142.2	0.3	0.5	0.7
0.2	ID08	1.06	0.096	1.3	149.9	0.3	0.4	0.6
0.3	ID01	1.64	0.010	2.6	20.5	3.0	5.0	7.0
0.3	ID02	2.13	0.021	3.5	58.0	1.4	2.3	3.2
0.3	ID03	0.82	0.029	1	16.9	1.8	3.0	4.2
0.3	ID04	1.86	0.051	3	121.4	0.6	1.0	1.3
0.3	ID05	1.42	0.059	2.2	100.2	0.5	0.9	1.2
0.3	ID06	0.96	0.076	1.3	66.6	0.5	0.9	1.3
0.3	ID07	0.89	0.096	1.15	69.8	0.5	0.8	1.1
0.3	ID08	1.22	0.116	1.8	155.2	0.3	0.5	0.7
0.3	ID09	1.06	0.144	1.5	152.2	0.3	0.4	0.6
0.4	ID01	1.14	0.010	1.8	8.5	5.0	8.4	11.8
0.4	ID02	1.91	0.020	3.5	41.0	1.7	2.9	4.1
0.4	ID03	2.14	0.030	4	72.1	1.1	1.9	2.6
0.4	ID04	0.81	0.049	1	15.1	2.0	3.3	4.7
0.4	ID05	1.68	0.060	3	101.8	0.6	1.0	1.4
0.4	ID06	0.87	0.078	1.15	32.2	1.0	1.7	2.4
0.4	ID07	1.49	0.098	2.6	141.3	0.4	0.7	0.9
0.4	ID08	0.93	0.116	1.3	60.4	0.6	1.0	1.3
0.4	ID09	1.31	0.126	2.2	146.9	0.3	0.6	0.8
0.4	ID10	1.02	0.145	1.5	96.1	0.4	0.7	0.9

3.5. PRELIMINARY EXPERIMENTS

Pure-current flow experiments

The combined wave-current flows used to study energy dissipation induced by vegetation were obtained by setting a steady flow in the flume and then overlapping the collinear waves with the characteristics specified in table 3.2. The steady flow conditions were achieved by setting the flow rate and the height of the sharp-crested weir at the end of the channel so that to obtain at the target mean current velocities. Free surface gradient Δs was measured in unvegetated bed condition by two ultrasonic gauges located at both ends of the test section at a distance of 6.7 m from each other. Measurements of the free surface profile (taken with ultrasonic gauges) and of the flow rate (from the electromagnetic flowmeter) were analyzed to check that the flow was indeed steady throughout the experiments. Results were compared with the theoretical free surface profile for a steady flow calculated as Citrini & Noseda (1987):

$$\Delta s = \frac{\Delta \mathrm{E}_b}{i - J} \tag{3.2}$$

where $\Delta \mathrm{E}_b$ is the gradient of specific energy with respect to the bed, i is the bed slope (which is equal to zero, being the channel non-tilted) and J is the head drop with respect to the bed.

In table 3.3 the theoretical and measured free surface profiles along the test section in condition of unvegetated bed are compared.

Table 3.3: theoretical and measured free surface profiles

Experimental conditions	Δs (measured) [mm]	Δs (predicted) [mm]
h40 – U1	-0.4	-0.1
h40 – U2	-0.5	-0.2
h40 – U3	-0.6	-0.4
h30 – U1	0.1	-0.1
h30 – U2	0.1	-0.2
h30 – U3	0.1	-0.4
h20 – U1	0.0	-0.1
h20 – U2	-0.1	-0.3
h20 – U3	-0.4	-0.6

A negative Δs means a decrease in water depth, that is the condition expected from theory (Citrini & Noseda, 1987). Measured Δs are comparable with theory and, being in the order of 0.5 mm, the free surface profile can be approximated as horizontal in the test section. Positive values obtained for h30 and h20 – U1 are considered as zero (negligible free surface gradient).

Pure-wave flow experiments

A series of 27 experiments with pure waves with the characteristics reported in table 3.2 were performed for each of the four densities considered in the present work and in condition of unvegetated bed. Dissipation coefficients $K_{D,pw}$ were calculated by removing from the dissipation obtained with vegetation the dissipation obtained in unvegetated bed condition for the same experimental conditions. Results are reported in table 3.4, with their 95% confidence intervals estimated from the linear regression and considering uncertainty propagation as explained later on. The dissipation coefficients of pure-waves were used as a benchmark to evaluate the impacts of following currents on meadow-induced wave dissipation.

Table 3.4: dissipation coefficients obtained in pure-wave conditions with the 95% confidence intervals. Each column corresponds to experiments performed with different vegetation density, respectively 251, 502, 669 and 1338 plants/m²

h [m]	TEST	Veg251 $K_{D,pw}$ [1/m²]	Veg502 $K_{D,pw}$ [1/m²]	Veg669 $K_{D,pw}$ [1/m²]	Veg1338 $K_{D,pw}$ [1/m²]
0.2	ID01	5.12 ± 2.91	5.91 ± 2.77	7.52 ± 2.41	11.19 ± 2.62
0.2	ID02	1.64 ± 0.85	2.38 ± 0.96	2.63 ± 0.84	3.91 ± 1.01
0.2	ID03	1.69 ± 0.66	2.28 ± 0.58	2.67 ± 0.54	3.91 ± 0.74
0.2	ID04	1.41 ± 0.57	1.93 ± 0.84	2.23 ± 0.63	3.32 ± 0.87
0.2	ID05	1.58 ± 0.66	2.77 ± 1.17	2.5 ± 0.75	3.82 ± 0.86
0.2	ID06	1.41 ± 0.56	2.24 ± 0.74	2.35 ± 0.64	3.51 ± 0.74
0.2	ID07	1.15 ± 0.32	1.61 ± 0.3	1.8 ± 0.32	2.92 ± 0.46
0.2	ID08	0.71 ± 0.45	1.21 ± 0.4	1.41 ± 0.47	2.43 ± 0.65
0.3	ID01	3.67 ± 4.69	4.19 ± 4.85	4.56 ± 4.61	5.48 ± 4.88
0.3	ID02	0.4 ± 4.69	0.75 ± 4.75	0.84 ± 4.97	2.18 ± 4.94
0.3	ID03	0.84 ± 0.8	1.12 ± 1.1	0.36 ± 0.69	1.56 ± 0.78
0.3	ID04	0.49 ± 0.61	0.7 ± 0.59	0.77 ± 0.73	1.4 ± 0.68
0.3	ID05	0.58 ± 0.45	0.71 ± 0.62	0.82 ± 0.48	1.3 ± 0.57
0.3	ID06	0.49 ± 0.47	0.57 ± 0.49	0.61 ± 0.46	0.94 ± 0.47
0.3	ID07	0.47 ± 0.17	0.56 ± 0.11	0.5 ± 0.2	0.85 ± 0.14
0.3	ID08	0.41 ± 0.18	0.5 ± 0.2	0.59 ± 0.21	0.9 ± 0.32
0.3	ID09	0.36 ± 0.13	0.5 ± 0.18	0.55 ± 0.17	0.78 ± 0.3
0.4	ID01	2.01 ± 3.26	1.96 ± 3.46	2.63 ± 3.21	3.43 ± 3.35
0.4	ID02	1.65 ± 3.13	2.12 ± 3.05	2.11 ± 3.3	2.58 ± 3.42
0.4	ID03	0.66 ± 3.23	0.91 ± 3.42	1.09 ± 3.31	1.32 ± 3.51
0.4	ID04	0.19 ± 0.35	0.29 ± 0.33	0.27 ± 0.4	0.37 ± 0.34
0.4	ID05	0.17 ± 0.31	0.32 ± 0.27	0.39 ± 0.33	0.6 ± 0.3
0.4	ID06	0.16 ± 0.25	0.25 ± 0.22	0.24 ± 0.28	0.32 ± 0.21
0.4	ID07	0.26 ± 0.23	0.36 ± 0.23	0.41 ± 0.19	0.58 ± 0.2
0.4	ID08	0.1 ± 0.22	0.12 ± 0.22	0.16 ± 0.23	0.17 ± 0.19
0.4	ID09	0.14 ± 0.15	0.2 ± 0.21	0.24 ± 0.18	0.38 ± 0.24
0.4	ID10	0.17 ± 0.11	0.25 ± 0.15	0.28 ± 0.16	0.32 ± 0.15

Combined wave-current flow in unvegetated bed condition experiments

Experiments were performed also in a condition of unvegetated bed in order to estimate the contribution of bed and side-walls friction to the total dissipation. Hence, dissipation coefficients calculated for unvegetated bed were subtracted from each corresponding test performed with the selected plant densities. Uncertainty on the estimation was propagated in the subtraction following Taylor (1997) formula:

$$\delta_{K_{D,wc}} = \delta_{K_{D,wc,veg0}} + \delta_{K_{D,wc,lr}} \tag{3.3}$$

where $\delta_{K_{D,wc}}$ is the uncertainty on the estimation of the dissipation coefficient and $\delta_{K_{D,wc,veg0}}$ and $\delta_{K_{D,wc,lr}}$ are the uncertainties estimated from linear regression for $K_{D,wc}$ for unvegetated bed and selected density respectively.

The results obtained are reported in table 3.5.

3.6. DATA ANALYSIS

Signals of free surface level η collected from wave gauges were processed to estimate wave dissipation coefficients. Waves were interpreted assuming linear theory from Dean & Dalrymple (1991) to be valid, even if the waves tested in the experiments don't fall in linear theory's applicability range in the Le Méhauté's diagram as shown in figure 3.9. Hence, the wave orbital velocity at canopy top U_c was obtained from linear wave theory, considering the measured wave height, whose calculation is explained below. Wave period was considered the same of the pure-wave case, as it has been observed that added current didn't have an influence on it. Current velocity was calculated by time-averaging over the experiments' duration the velocity obtained from the flow rate measured by the electromagnetic flow meter, knowing flume's geometrical properties and water depth from Vernier scale's readings. Water kinematic viscosity and density were calculated from water temperature measured before each test.

The first steps of data analysis aimed to remove the parts of the signals affected by wave reflection and the transient at the beginning, induced respectively by the sharp-crested weir and the wavemaker. They have been performed as follows:

- Signals have been detrended to remove the effect of water depth variations.
- Signals have been cut 5 s before the theoretical arrival time of the first reflected wave to each wave gauge, calculated assuming linear wave theory.
- A reference wave height has been calculated from a reference timespan including the last 5 wave periods of the cut signal.
- Wave heights of each wave period antecedent to the reference timespan have been compared with the reference wave height with a tolerance of 10%. Procedure stopped with the first wave period with wave height not belonging to the reference wave height range. This became the starting point of the cut signal.

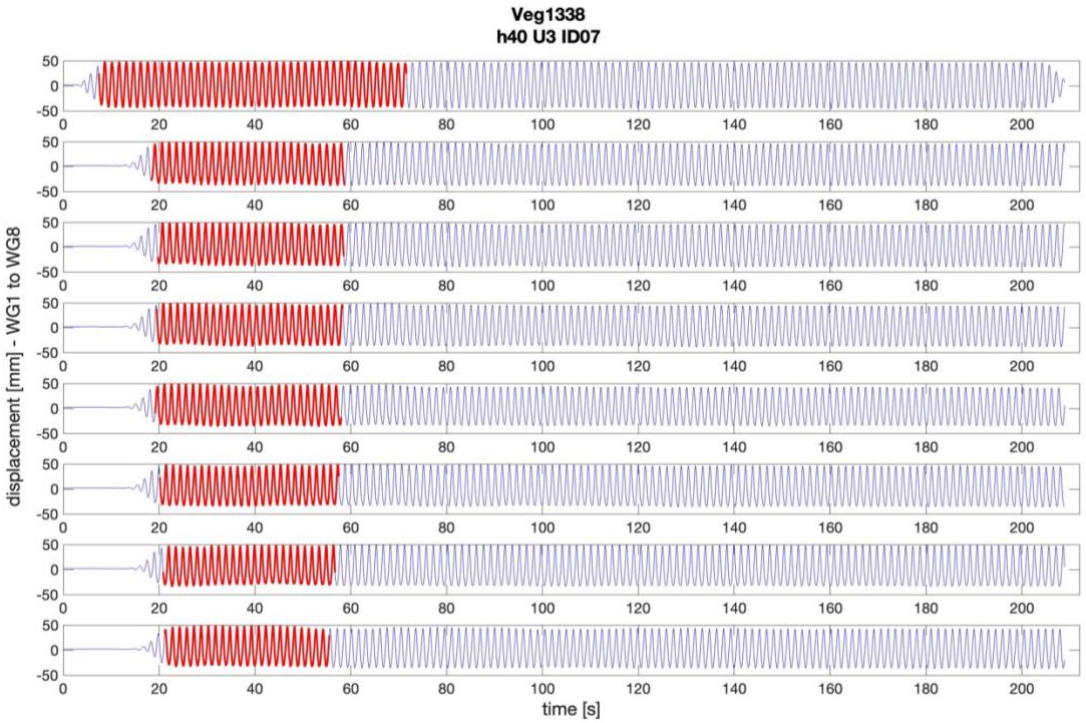

Figure 3.10: signals obtained for each WG (sorted from 1 to 8 from top to bottom) during one experiments. The part highlighted is red is the one analyzed to obtain the dissipation coefficient

Wave height H has been calculated from the root mean square of the signals (η_{rms}) as indicated by Schaefer & Nepf (2022):

$$\mathrm{H} = \sqrt{2} * 2\eta_{rms} \tag{3.4}$$

Dissipation coefficients $K_{D,wc}$ have been obtained by interpolating experimental data with the wave attenuation model proposed by Schaefer & Nepf (2022):

$$a_w(x) = \frac{a_0}{1 + K_{D,wc} a_{w,0} x} \tag{3.5}$$

that rewriting becomes:

$$\frac{a_{w,0} - a_w(x)}{a_w(x)} = K_{D,wc} a_{w,0} x \tag{3.6}$$

Comparing equation (3.6) with a linear regression as $y = mx + q$, where x is the independent variable, y the dependent variable, m the slope and q the intercept, it follows:

$$m = K_{D,wc} a_{w,0} \tag{3.7}$$

Knowing that wave amplitude is half of the wave height it is possible to obtain the wave dissipation coefficient:

$$K_{D,wc} = 2\frac{m}{H_0} \tag{3.8}$$

where $H_0 = H(WG2)$.

It should be pointed out that linear regression has been performed with the free intercept instead of forcing it to zero to better adapt model to experimental errors. All the intercepts fell in a limited range around zero.

Table 3.5: dissipation coefficients obtained in combined wave-current conditions with the 95% confidence intervals

h20-U1	Veg251 [m^{-2}]	Veg502 [m^{-2}]	Veg669 [m^{-2}]	Veg1338 [m^{-2}]
ID01	2.17 ± 2.81	3.65 ± 2.80	5.07 ± 2.62	6.82 ± 3.44
ID02	0.23 ± 0.37	0.79 ± 0.41	1.06 ± 0.29	2.28 ± 0.35
ID03	0.38 ± 0.35	0.72 ± 0.42	0.97 ± 0.45	2.03 ± 0.21
ID04	0.40 ± 0.51	0.75 ± 0.40	1.02 ± 0.49	1.91 ± 0.80
ID05	1.93 ± 4.86	2.22 ± 5.34	0.69 ± 4.05	4.13 ± 5.32
ID06	1.05 ± 1.43	1.39 ± 1.30	1.76 ± 0.96	2.64 ± 0.94
ID07	0.20 ± 0.24	0.45 ± 0.25	0.61 ± 0.20	1.21 ± 0.36
ID08	0.15 ± 0.26	0.37 ± 0.20	0.41 ± 0.34	1.15 ± 0.24

h30-U1	Veg251 [m^{-2}]	Veg502 [m^{-2}]	Veg669 [m^{-2}]	Veg1338 [m^{-2}]
ID01	1.35 ± 1.40	1.88 ± 0.83	2.12 ± 1.20	4.27 ± 1.35
ID02	0.65 ± 1.30	1.18 ± 1.49	1.22 ± 1.58	3.02 ± 1.01
ID03	0.37 ± 0.43	0.65 ± 0.49	0.69 ± 0.49	1.63 ± 0.25
ID04	0.12 ± 0.23	0.32 ± 0.27	0.39 ± 0.23	1.12 ± 0.14
ID05	0.17 ± 0.14	0.30 ± 0.20	0.44 ± 0.13	1.01 ± 0.07
ID06	0.13 ± 0.10	0.19 ± 0.13	0.22 ± 0.09	0.72 ± 0.05
ID07	0.10 ± 0.10	0.14 ± 0.15	0.18 ± 0.09	0.57 ± 0.10
ID08	0.10 ± 0.15	0.33 ± 0.46	0.24 ± 0.14	0.68 ± 0.10
ID09	0.11 ± 0.28	0.26 ± 0.42	0.18 ± 0.25	0.52 ± 0.15

h40-U1	Veg251 [m^{-2}]	Veg502 [m^{-2}]	Veg669 [m^{-2}]	Veg1338 [m^{-2}]
ID01	0.42 ± 1.95	0.89 ± 2.11	1.05 ± 2.13	0.80 ± 2.69
ID02	0.26 ± 1.62	0.46 ± 1.74	0.69 ± 1.87	0.97 ± 1.87
ID03	0.16 ± 0.81	0.26 ± 0.89	0.51 ± 0.88	0.65 ± 0.83
ID04	0.06 ± 0.19	0.10 ± 0.18	0.18 ± 0.22	0.17 ± 0.23
ID05	0.06 ± 0.17	0.15 ± 0.18	0.22 ± 0.21	0.49 ± 0.24
ID06	0.06 ± 0.08	0.08 ± 0.09	0.09 ± 0.12	0.15 ± 0.16
ID07	0.07 ± 0.10	0.12 ± 0.07	0.14 ± 0.06	0.35 ± 0.09
ID08	0.04 ± 0.07	0.06 ± 0.09	0.08 ± 0.09	0.18 ± 0.09
ID09	0.04 ± 0.06	0.07 ± 0.06	0.11 ± 0.06	0.25 ± 0.12
ID10	-0.01 ± 0.11	0.02 ± 0.11	0.03 ± 0.12	0.17 ± 0.13

h20-U2	Veg251 [m^{-2}]	Veg502 [m^{-2}]	Veg669 [m^{-2}]	Veg1338 [m^{-2}]
ID01	2.93 ± 2.33	4.31 ± 2.45	5.30 ± 2.47	8.17 ± 3.99
ID02	0.36 ± 0.58	0.93 ± 0.62	1.11 ± 0.54	1.94 ± 0.54
ID03	0.34 ± 0.52	0.68 ± 0.55	0.77 ± 0.49	1.54 ± 0.42
ID04	0.19 ± 0.35	0.56 ± 0.26	0.77 ± 0.29	1.44 ± 0.66
ID05	0.26 ± 2.13	0.46 ± 2.29	0.18 ± 2.32	0.97 ± 1.94
ID06	0.51 ± 1.38	1.14 ± 1.56	1.13 ± 1.48	1.56 ± 1.23
ID07	0.20 ± 0.25	0.73 ± 0.26	0.52 ± 0.11	1.24 ± 0.22
ID08	0.35 ± 0.23	0.54 ± 0.17	0.50 ± 0.15	1.26 ± 0.23

h30-U2	Veg251 [m^{-2}]	Veg502 [m^{-2}]	Veg669 [m^{-2}]	Veg1338 [m^{-2}]
ID01	1.64 ± 1.95	1.93 ± 1.03	2.09 ± 1.46	3.59 ± 1.75
ID02	0.51 ± 1.05	0.83 ± 1.23	1.18 ± 1.30	1.55 ± 0.58
ID03	0.43 ± 0.54	0.60 ± 0.53	0.78 ± 0.61	1.21 ± 0.39
ID04	0.15 ± 0.22	0.25 ± 0.25	0.40 ± 0.26	0.88 ± 0.14
ID05	0.18 ± 0.14	0.27 ± 0.18	0.42 ± 0.15	0.76 ± 0.07
ID06	0.11 ± 0.12	0.13 ± 0.15	0.21 ± 0.19	0.52 ± 0.11
ID07	0.14 ± 0.12	0.12 ± 0.15	0.18 ± 0.14	0.40 ± 0.10
ID08	0.08 ± 0.08	0.15 ± 0.10	0.23 ± 0.11	0.51 ± 0.06
ID09	0.09 ± 0.07	0.11 ± 0.07	0.18 ± 0.07	0.35 ± 0.04

h40-U2	Veg251 [m^{-2}]	Veg502 [m^{-2}]	Veg669 [m^{-2}]	Veg1338 [m^{-2}]
ID01	1.38 ± 2.03	1.94 ± 2.16	2.51 ± 1.55	2.65 ± 2.21
ID02	0.50 ± 1.38	0.66 ± 2.00	0.83 ± 1.60	1.05 ± 1.86
ID03	0.23 ± 0.95	0.34 ± 0.97	0.54 ± 0.98	0.68 ± 0.95
ID04	0.17 ± 0.29	0.25 ± 0.28	0.28 ± 0.28	0.38 ± 0.27
ID05	0.09 ± 0.13	0.17 ± 0.12	0.19 ± 0.13	0.45 ± 0.17
ID06	0.09 ± 0.15	0.12 ± 0.18	0.13 ± 0.2	0.21 ± 0.24
ID07	0.07 ± 0.09	0.11 ± 0.09	0.14 ± 0.10	0.32 ± 0.12
ID08	0.06 ± 0.10	0.12 ± 0.11	0.10 ± 0.11	0.20 ± 0.11
ID09	0.06 ± 0.06	0.09 ± 0.06	0.12 ± 0.06	0.22 ± 0.13
ID10	0.06 ± 0.08	0.06 ± 0.09	0.09 ± 0.08	0.15 ± 0.10

h20-U3	Veg251 [m^{-2}]	Veg502 [m^{-2}]	Veg669 [m^{-2}]	Veg1338 [m^{-2}]
ID01	0.64 ± 4.35	0.82 ± 4.82	1.85 ± 4.79	7.23 ± 5.62
ID02	0.41 ± 0.62	0.87 ± 0.72	0.95 ± 0.55	1.62 ± 0.70
ID03	0.44 ± 0.51	0.74 ± 0.50	0.80 ± 0.43	1.69 ± 0.57
ID04	0.29 ± 0.48	0.67 ± 0.61	0.83 ± 0.58	1.48 ± 0.60
ID05	0.24 ± 1.69	0.80 ± 1.76	0.68 ± 1.36	2.59 ± 1.77
ID06	0.68 ± 0.88	0.67 ± 1.15	0.35 ± 0.80	0.91 ± 0.93
ID07	0.24 ± 0.35	0.47 ± 0.33	0.59 ± 0.30	1.44 ± 0.44
ID08	0.27 ± 0.44	0.41 ± 0.45	0.42 ± 0.45	1.55 ± 0.46

h30-U3	Veg251 [m^{-2}]	Veg502 [m^{-2}]	Veg669 [m^{-2}]	Veg1338 [m^{-2}]
ID01	0.83 ± 2.92	1.23 ± 2.06	1.35 ± 2.54	1.51 ± 2.38
ID02	0.01 ± 0.94	0.48 ± 1.17	0.51 ± 1.00	0.95 ± 0.63
ID03	0.35 ± 0.52	0.56 ± 0.60	0.87 ± 0.54	1.31 ± 0.35
ID04	0.07 ± 0.21	0.21 ± 0.21	0.35 ± 0.17	0.70 ± 0.14
ID05	0.22 ± 0.21	0.23 ± 0.18	0.37 ± 0.22	0.57 ± 0.16
ID06	0.19 ± 0.22	0.16 ± 0.28	0.28 ± 0.25	0.41 ± 0.12
ID07	0.09 ± 0.17	0.10 ± 0.18	0.17 ± 0.18	0.37 ± 0.11
ID08	0.07 ± 0.14	0.12 ± 0.21	0.20 ± 0.16	0.39 ± 0.08
ID09	0.09 ± 0.08	0.10 ± 0.08	0.18 ± 0.06	0.32 ± 0.06

h40-U3	Veg251 [m^{-2}]	Veg502 [m^{-2}]	Veg669 [m^{-2}]	Veg1338 [m^{-2}]
ID01	0.03 ± 2.55	0.40 ± 2.82	0.13 ± 2.26	0.09 ± 3.13
ID02	-0.19 ± 1.79	0.38 ± 2.17	0.20 ± 1.99	0.11 ± 1.99
ID03	-0.01 ± 0.85	0.08 ± 1.07	0.24 ± 1.17	0.37 ± 1.15
ID04	-0.06 ± 0.22	0.09 ± 0.22	0.13 ± 0.24	0.42 ± 0.28
ID05	0.10 ± 0.19	0.26 ± 0.17	0.23 ± 0.18	0.44 ± 0.25
ID06	0.13 ± 0.11	0.17 ± 0.14	0.12 ± 0.14	0.21 ± 0.23
ID07	0.08 ± 0.09	0.13 ± 0.09	0.14 ± 0.11	0.31 ± 0.13
ID08	0.08 ± 0.05	0.11 ± 0.10	0.12 ± 0.11	0.18 ± 0.14
ID09	0.04 ± 0.15	0.09 ± 0.16	0.10 ± 0.17	0.19 ± 0.17
ID10	0.09 ± 0.09	0.12 ± 0.10	0.13 ± 0.11	0.20 ± 0.14

4. RESULTS AND DISCUSSION

4.1. K_D PREDICTION BASED ON MODEL BY LOSADA ET AL. (2016)

The wave attenuation calculated from wave height measurements is compared with dissipation coefficients predicted using the wave dissipation model for combined wave-current flows proposed by Losada et al. (2016). The model defines a dissipation coefficient β, combining equations (2.24) and (2.36), as:

$$\beta_{wc} = K_{D,wc}\frac{H_0}{2} \tag{4.1}$$

Losada et al. (2016) considered a uniform and irrotational wave-current field, incorporating the effect of plants bending and motion into the drag coefficient. They obtained an empirical formulation to quantify the effect of this interaction between flow and canopy by fitting experimental data (see equation 2.12).

The length scale used in equation (2.26) to quantify wave dissipation is the deflected height h_D, that represents the actual blade area that resists to the flow, after plants bending. In their study, it was measured from images recorded during experiments. In the absence of direct measurements in the present study, the deflected height has been approximated as function of current velocity that produces reconfiguration using the empirical formulation proposed by Schaefer & Nepf (2022):

$$\frac{h_D - l_r}{l_b} = 1 - \frac{1 - Ca_c^{-\frac{1}{4}}}{1 + 4Ca_c^{-\frac{3}{5}} + 8Ca_c^{-2}} \tag{4.2}$$

In figure 5.1 dissipation coefficients predictions based on model developed by Losada et al. (2016) are shown together with their 95% confidence intervals. The range in x axis has been reduced in each figure with error bars to help visualization

of data. This was done even though some confidence intervals exceed the x range being used. Uncertainty has always been calculated as the 95% confidence interval on the linear regression.

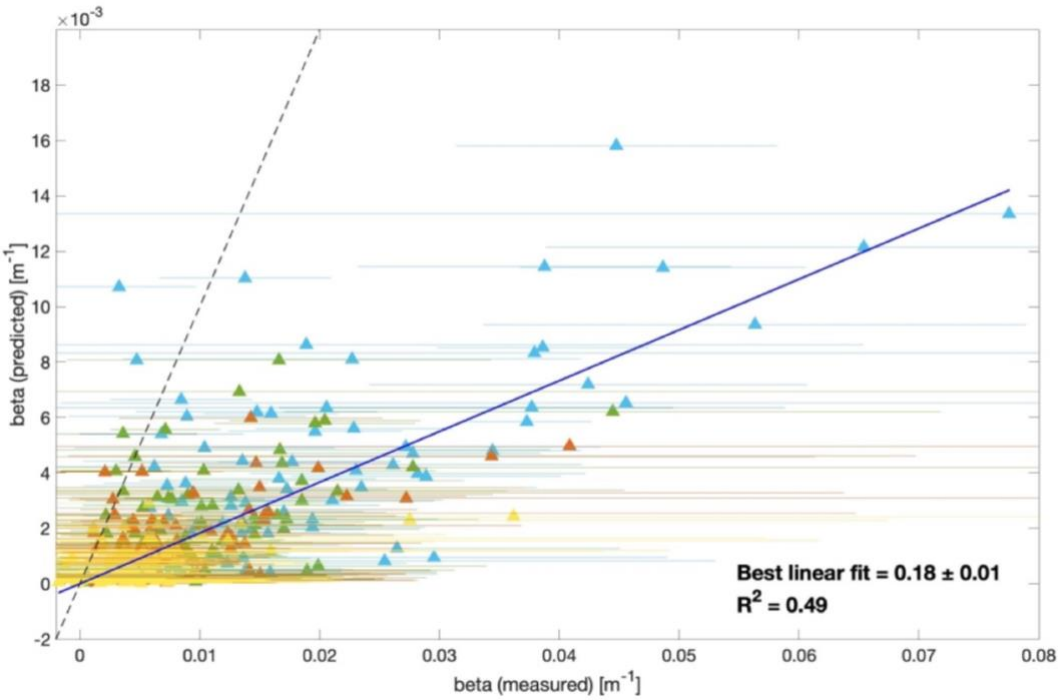

Figure 4.1: measured wave dissipation coefficient versus predicted wave dissipation coefficient using model by Losada et al. (2016). The dashed grey line denotes 1:1 agreement, the blue solid denotes best linear fit of measured wave dissipation coefficient. Cyan symbols denote Veg1338, green symbols denote Veg669, red symbols denote Veg502 and yellow symbol denote Veg251.

The model strongly underestimates wave attenuation: a linear fit of β_{wc} (predicted) versus β_{wc} (measured) yields a slope of 0.18 ± 0.01. Drag coefficient proposed by Losada et al. (2016) is optimized for their experiments that have been performed with different conditions in respect to the ones realized in the present work. Submergence ratio varies between 0.5 and 1, with cases in which vegetation is even higher than the water column, and some biomechanical properties are different. Wave heights are in general higher than the ones used in the present work and vegetation conditions are considered as dense, unlike the present work.

A slightly better prediction (figure 5.2) of wave dissipation has been obtained using equation (2.3) to approximate the drag coefficient and the interaction flow-plant.

Specifically, β_{wc} (predicted) $= (1.75 \pm 0.16)\ \beta_{wc}$ (measured). Drag coefficient has been considered constant along the meadow length, neglecting any increase with distance related to the reduction of wave amplitude in test section. This assumption yields for all the models analyzed.

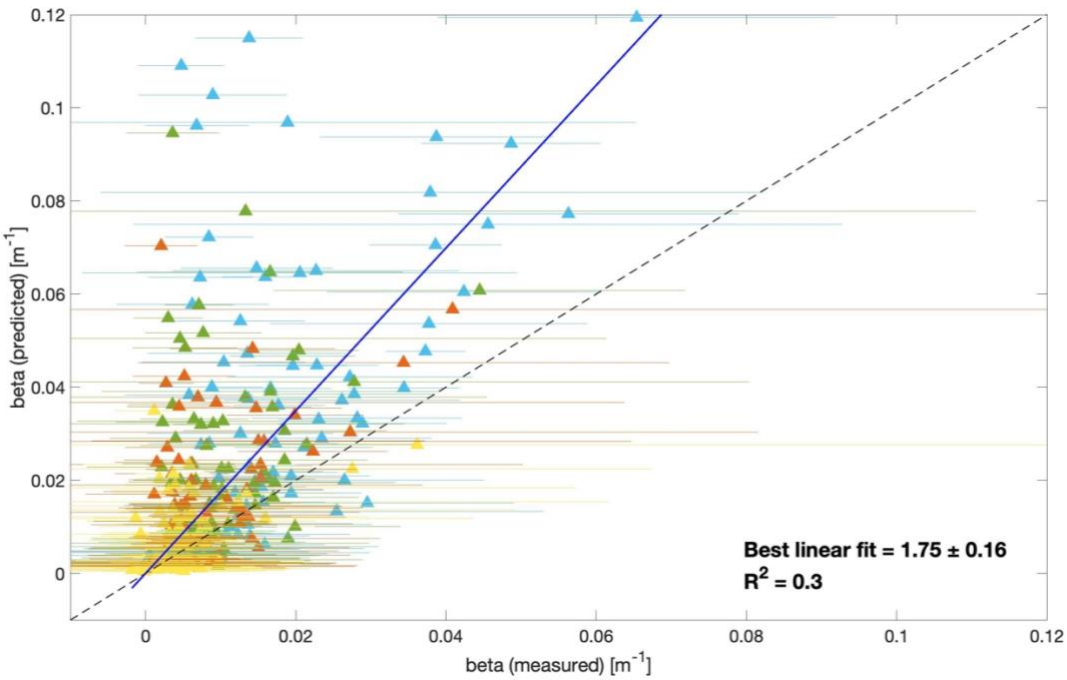

Figure 4.2: measured wave dissipation coefficient versus predicted wave dissipation coefficient using model by Losada et al. (2016) with the formulation for drag coefficient introduced in Schaefer & Nepf (2022). The dashed grey line denotes 1:1 agreement, the blue solid denotes best linear fit of measured wave dissipation coefficient. Cyan symbols denote Veg1338, green symbols denote Veg669, red symbols denote Veg502 and yellow symbol denote Veg251.

Despite the applied correction on the drag coefficient, the model overestimates the dissipation coefficients by 75%. This result is consistent with the prediction made by Schaefer & Nepf (2022). They compared their measured wave dissipation coefficients with the theoretical model they developed, using the deflected height in place of the effective meadow length as length scale for vegetation in equation (2.37) and the formulation of equation (2.3) for drag coefficient, obtaining an overestimation of wave dissipation by about 70% (see figure 5a of Schafer & Nepf, 2022). This similarity suggests that use of deflected length as vegetation length scale leads to an overestimation of wave dissipation, because it does not account for the wave-induced blade reconfiguration and for the influence of current on it.

4.2. K_D PREDICTION BASED ON MODEL BY SCHAEFER AND NEPF (2022)

Predictions of dissipation coefficients in combined wave-current conditions based on model by Schaefer & Nepf (2022) are compared with experimental results in *figure 5.3.* The effective meadow height $l_{e,m,wc}$ was estimated using wave conditions measured just before the test section, at WG2, neglecting changes in Ca_{wc} and KC that occurs with wave amplitude attenuation along the meadow.

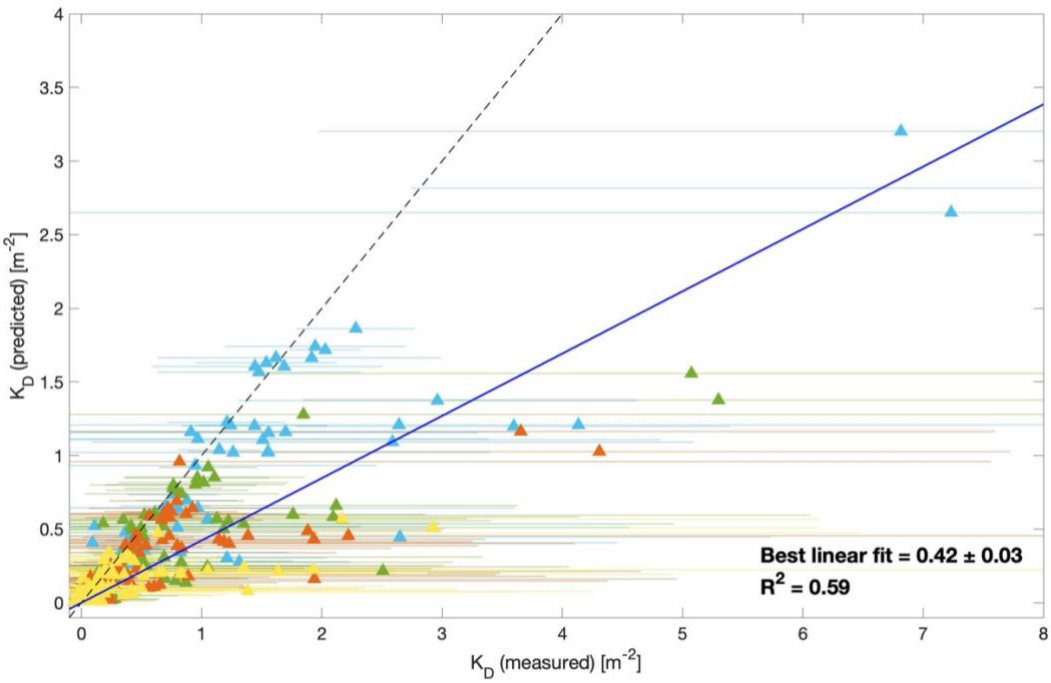

Figure 4.3: measured wave dissipation coefficient versus predicted wave dissipation coefficient using model by Schaefer & Nepf (2022). The dashed grey line denotes 1:1 agreement, the blue solid denotes best linear fit of measured wave dissipation coefficient. Cyan symbols denote Veg1338, green symbols denote Veg669, red symbols denote Veg502 and yellow symbol denote Veg251.

As explained in *Chapter 2,* in Schaefer & Nepf (2022) model the time-averaged in-canopy velocity U_1 replaces the time-averaged current velocity U_c. Flow velocity is reduced inside meadows and the use of the undisturbed time-average current velocity would lead to an overestimation of the degree of reconfiguration and drag reduction. U_1 has been calculated using for the mean deflected meadow height h_D the empirical relation introduced above in equation (4.2).

The model underestimates the wave energy dissipation measured by around 60%. Specifically, $K_{D,wc}(\text{predicted}) = (0.42 \pm 0.03)\, K_{D,wc}(\text{measured})$. This behavior is evident in particular for the cases in which $K_{D,wc}$ is higher, namely when submergence ratio is greater and wave heights and current velocity are lower. These data are quite noisy, and it may be because of issues in data acquisition in certain conditions due to the experimental setup used in the present work. Moreover, being the model based on a single vegetation density of 950 plants/m^2, it works better (see figure 4.4) with the two vegetation densities (669 and 1338 plants/m^2) more similar to the one tested by Schaefer & Nepf (2022). Data that deviates more from the model are the one characterized by lower wave height and lower Keulegan-Carpenter number. In general, th wave period of data that more deviates from the model is lower than 1.5 s, while Schaefer & Nepf (2022) used a wave period of 2 s in all their experiments.

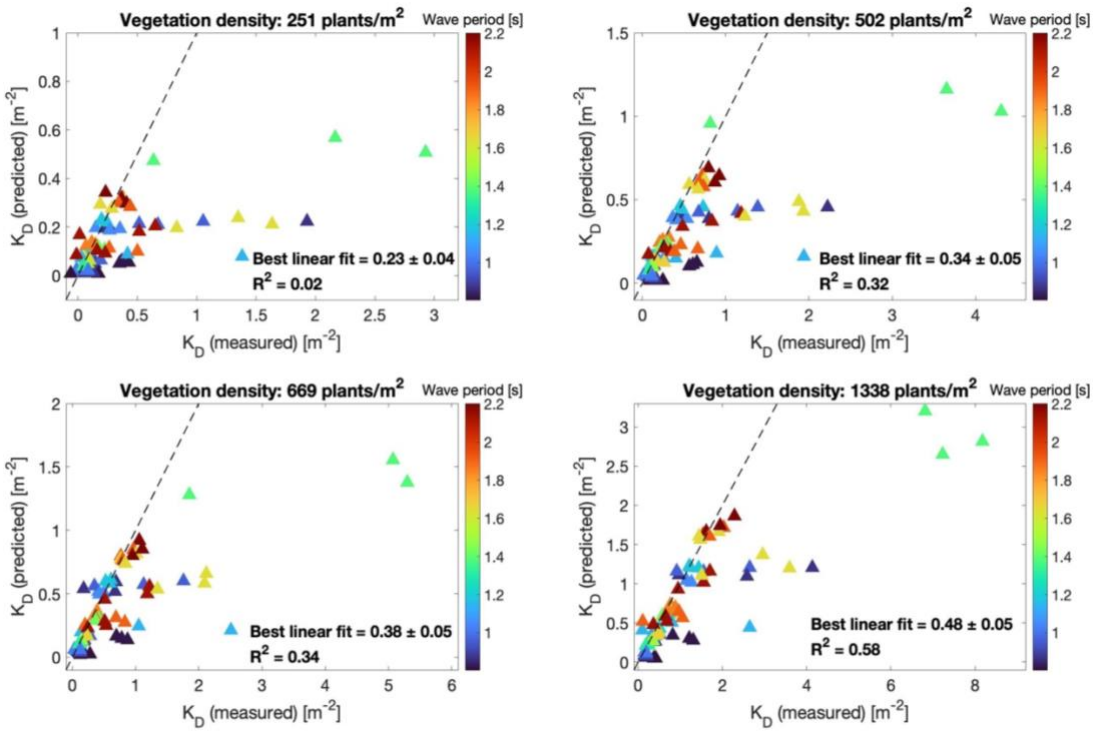

Figure 4.4: measured wave dissipation coefficient versus predicted wave dissipation coefficient using model by Schaefer & Nepf (2022) as function of vegetation density. The dashed grey lines denote 1:1 agreement. Cyan symbols denote Veg1338, green symbols denote Veg669, red symbols denote Veg502 and yellow symbol denote Veg251.

Some corrections have been performed to better adapt the model to experimental results and improve wave dissipation prediction. First, all the tests with $KC < 30$ have been neglected in the analysis (see figure 4.5 top left panel). Schaefer & Nepf (2022) approximated drag coefficient in combined wave-current conditions with the drag coefficient in pure-wave conditions calculated with equation (2.3), because current impact was negligible in their experimental conditions, based on Sarpkaya & Storm (1985). In the present work, the drag coefficients of experiments in which $KC < 30$ may be influenced by the presence of a current and cannot be considered equal to the case of pure-wave flow. These values contribute significantly to underestimate $K_{D,wc}$, so they are neglected in the comparison with the model and thus the correspondence improves. Second, the moment of inertia of the plants was multiplied by a factor that allowed to correct the blades curling observed (see figure 4.5 top rigth panel). Due to curling, blades' length is lower than the one expected from straight blades (see figure 3.7). The increase in plants' stiffness by modifying the moment of inertia in the model allows to better reproduce the experimental behaviour of mimic vegetation characterized by curled blades. More rigid plants deflect less under waves and currents, hence the degree of reconfiguration is lower and the dissipation increases becoming more similar to measured wave attenuation, due to the increased relative velocity. Specifically, curled blades have lower flexible length, and it has been observed that their bending during experiments was reduced. This behaviour has been modelled by increasing plants rigidity by a factor of 8. The factor came out from a set of dedicated tests wherein deflected length was measured on plants with curled blades and plants with straight blades.

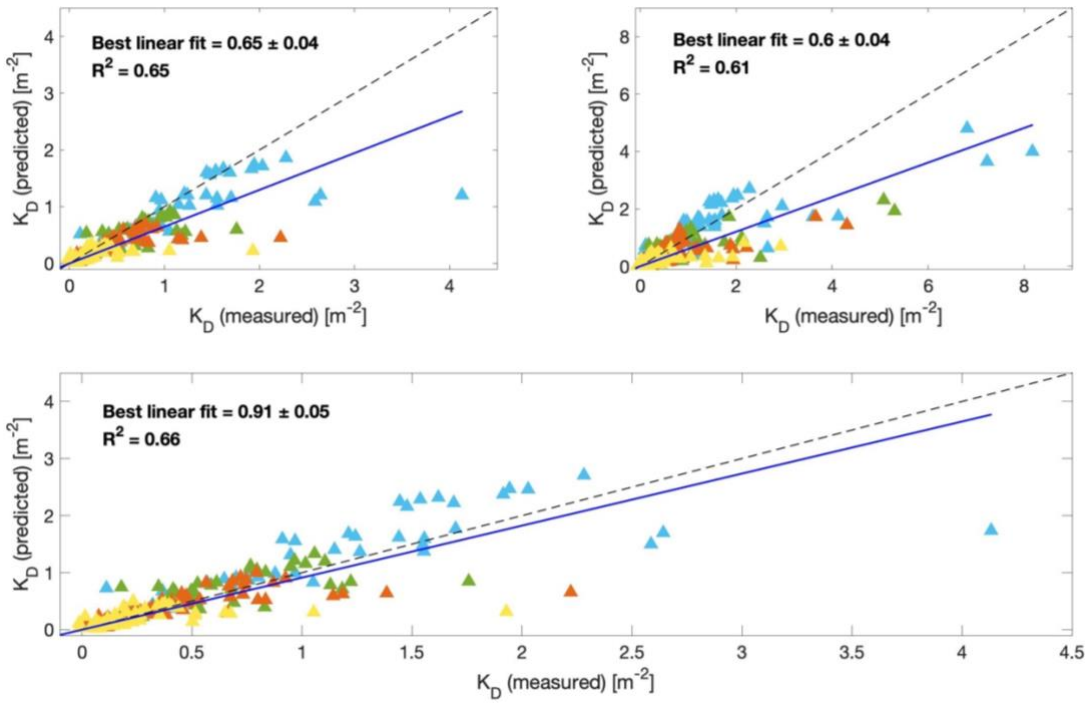

Figure 4.5: measured wave dissipation coefficient versus predicted wave dissipation coefficient using model by Schaefer & Nepf (2022). Top left graph represents the comparison between experiments with KC>30 and the model; top right graph represents the comparison between all experiments and the model in which plants' rigidity has been corrected; bottom graph represents the comparison between experiments with KC>30 and the model in which plants' rigidity has been corrected. The dashed grey line denotes 1:1 agreement, the blue solid denotes best linear fit of measured wave dissipation coefficient. Cyan symbols denote Veg1338, green symbols denote Veg669, red symbols denote Veg502 and yellow symbol denote Veg251.

Combining the two corrections described before (figure 4.5, bottom panel) the correspondence definitely improves. Specifically, the corrected model underestimates experimental results by only 10%, that is an acceptable value, indicating a good agreement between experimental data and the physical model proposed by Schaefer & Nepf (2022). It is still evident that experiments with the highest wave dissipation coefficients measured are the ones that model describes worst. As mentioned above, these measurements are quite noisy, and this can be related to the influence of wave period in wave dissipation. In their experiments wave period was always equal to $2\ s$, while in the present work it ranges between $0.81\ s$ and $2.20\ s$, and the lowest values are the furthest from the model, as it is possible to observe in figure 4.4.

4.3. INFLUENCE OF CURRENT ON MEASURED WAVE ATTENUATION

The measured dissipation coefficients in combined wave-current conditions $K_{D,wc}$ have been normalized by the dissipation coefficients for the corresponding pure-wave cases $K_{D,pw}$. Results for the different meadow densities are shown as function of the dimensionless number U_c/U_w in figure 4.6.

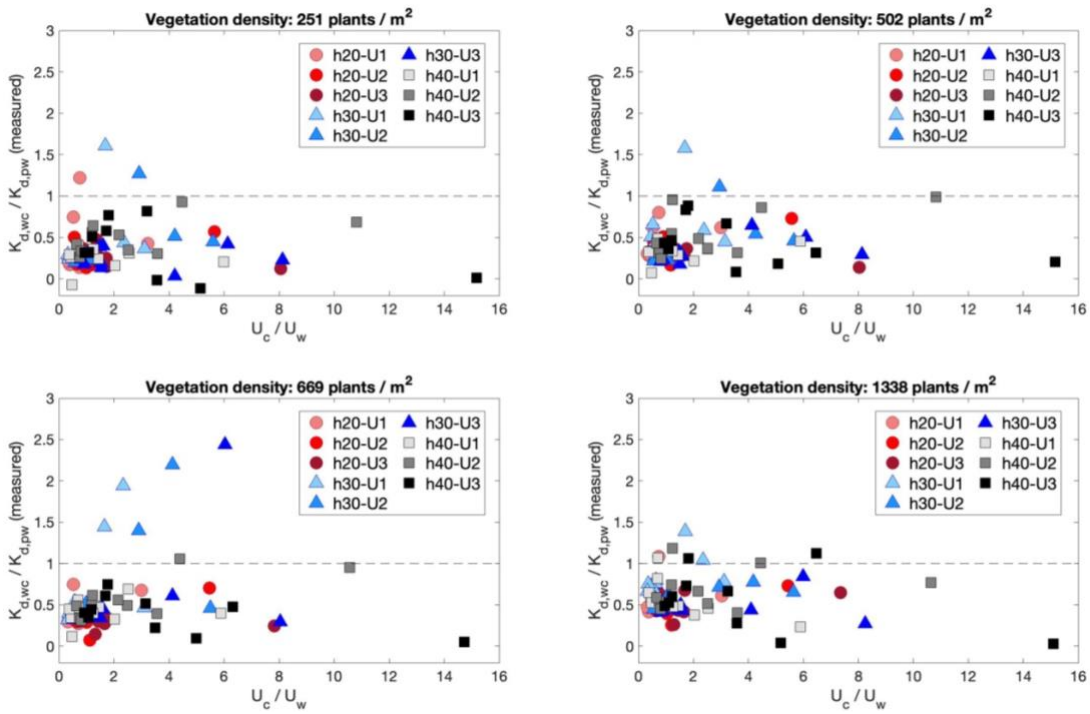

Figure 4.6: measured wave dissipation coefficient $K_{D,wc}$ for wave-current flows normalized by dissipation coefficients for pure wave conditions $K_{D,pw}$, with the same wave amplitude at the meadow leading edge, as a function of the dimensionless number U_c / U_w. The dashed grey line denotes $K_{D,wc}$= $K_{D,pw}$

In general, the addition of a following current decreases the wave dissipation. This means that the main impact of a current on the flexible vegetation used in the present work is to induce blade deflection. Vegetation deflecting reduces frontal area that resists to the flow, reducing hydrodynamic drag and, in turn, wave energy dissipation. The ratio between dissipation coefficient in combined wave-current and pure-wave conditions is observed to slightly increase with vegetation density: cluster of points in the region $2 < U_c/U_w < 4$ is shifted up by a small amount for each increase in density, meaning that the reduction in frontal area caused by the

following current is more relevant in less dense canopies. This effect has been quantified by computing the average $K_{D,wc}/K_{D,pw}$, reported with the standard deviation, for each vegetation density, respectively Veg251, Veg502, veg669 and Veg1338: 0.35 ± 0.28, 0.43 ± 0.24, 0.51 ± 0.40 and 0.59 ± 0.24.

Results are in agreement with what has been observed by Paul et al. (2012) and Losada et al. (2016). Paul et al. (2012) performed a series of flume experiments with flexible submerged vegetation with $U_c/U_w < 0.5$ (Zhang & Nepf, 2021) and obtained a reduced wave dissipation of about 30% when following currents are added to waves. Losada et al. (2016) performed a series of experiments with $0.5 < U_c/U_w < 1.4$ and obtained that a following always reduces wave dissipation compared to a pure-wave case. Results partially agree with Schaefer & Nepf (2022), that observed a negligible impact in adding a weak current ($U_c/U_w < 0.5$) and a decrease in dissipation coefficient compared to pure-wave case adding stronger currents ($U_c/U_w > 0.5$), with a clear decreasing trend, as shown in figure 2.2. They obtained these results performing experiments with flexible mimic plants composed by 6 blades and with a vegetation density of $950\ \text{plants/m}^2$, corresponding to a blade density of $5700\ \text{blades/m}^2$. In terms of blade density, Veg1338 is the only dataset of the present work similar to the one of Schaefer & Nepf (2022), corresponding to a blade density of $5352\ \text{blades/m}^2$. For Veg1338 wave dissipation has been reduced on average of about 41% when a current has been added. This is consistent with Schaefer & Nepf (2022) that observed a 40% reduction in wave dissipation due to current effect for $U_c/U_w > 0.5$. Blade density may be one of the parameters that create mismatch in $K_{D,wc}/K_{D,pw}$ as function of U_c/U_w between the present work and the research carried out by Schaefer & Nepf (2022). For the ratios between dissipation coefficient in combined wave-current and pure-wave conditions obtained in the present work no specific trends can be observed as function of U_c/U_w. $K_{D,wc}/K_{D,pw}$ is always lower than one for $U_c/U_w < 0.5$, in contrast to what has been observed in Schaefer & Nepf (2022). This could be explained by the different wave heights and wave periods involved in the experiments with $U_c/U_w < 0.5$: in the present work wave heights are greater than 5 cm and wave periods ranges from 0.9 s to 1.5 s, while Schaefer and & Nepf (2022) used wave heights lower than 4 cm and a single wave period of 2 s. For

$U_c/U_w > 0.5$ there is a weak decreasing trend of $K_{D,wc}/K_{D,pw}$, apart from some isolated tests in which current impact is negligible or even contributes to increase wave dissipation. The latter mainly belong to experiments in which KC is very low and results may be affected by other forces not negligible compared to hydrodynamic drag.

Moreover, still in contrast with what observed by Schaefer & Nepf (2022) in figure 2.2, no specific trends are present in figure 5.7, where the ratios between wave attenutaion in wave-current and pure-wave conditions as function of the wave Cauchy number Ca_w, are reported. This means that there is no evidence that in the present work the impact of a following current on wave dissipation depends on wave characteristics. Increasing Ca_w, which in the experiments means increasing U_w, the ratio $K_{D,wc}/K_{D,pw}$ does not vary, suggesting that the relative importance between blade reconfiguration and increasing of in-canopy velocity remains constant.

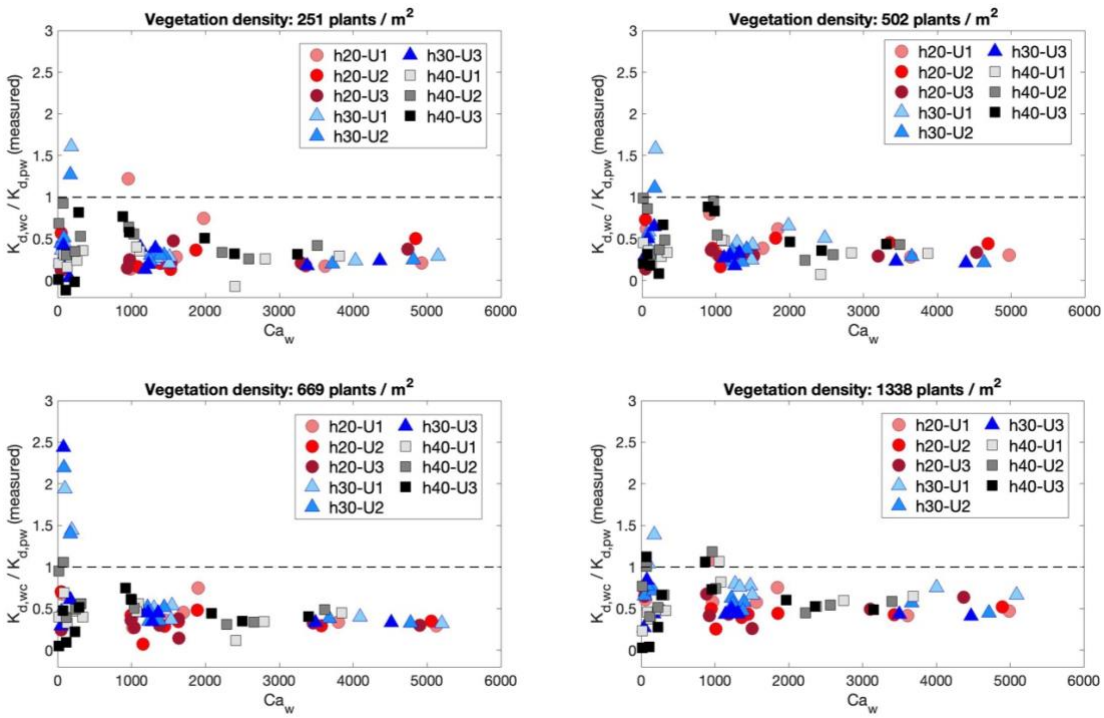

Figure 4.7: : measured wave dissipation coefficient $K_{D,wc}$ for wave-current flows normalized by dissipation coefficients for pure wave conditions $K_{D,pw}$, with the same wave amplitude at the meadow leading edge, as a function of the wave Cauchy number Ca_{wc}. The dashed grey line denotes $K_{D,wc} = K_{D,pw}$

4.4. EFFECT OF GOVERNING PARAMETERS ON WAVE ATTENUATION

Wave attenuation in combined wave-current conditions depends on blades reconfiguration. Flexible blades move passively under small-excursion waves reducing relative velocity between plant and water and thus reducing hydrodynamic drag (Lei & Nepf 2019b). Current impacts reconfiguration by deflecting blades and by limiting their wave-induce motion: the first reduces vegetation area exposed to the flow and thus drag, the latter dampen blade motion, increasing relative velocity between flow and plants (Schaefer & Nepf, 2022). Currents contribute to increase total in-canopy velocity and thus drag. Hence, hydrodynamic drag and blade reconfiguration are related and not independent to each other. Moreover, wave attenuation depends on vegetation density. More plants mean increased vegetation area exposed to the flow and thus higher wave dissipation.

Summing up, $K_{D,wc}$ depend on three main parameters:

$$K_{D,wc} \sim f\left(C_{D,wc}\right) f\left(a_v\right) f\left(l_{e,m,wc}\right) \tag{4.3}$$

$C_{D,wc}$ models the interaction between flow and a single plant in terms of resistance produced against the flow and, assuming it equal to the pure-wave case, is proportional to KC following equation (2.3); a_v describes the effect of vegetation density on wave dissipation; $l_{e,m,wc}$ models the interaction between flow and canopy, namely blade reconfiguration, and depends on the wave-current Cauchy number Ca_{wc} following equation (2.15).

In Schaefer & Nepf (2022) $K_{D,wc} \sim {Ca_{wc}}^{-0.41}$ for a submergence ratio equal to 0.5 and $K_{D,wc} \sim {Ca_{wc}}^{-0.37}$ for a submergence ratio equal to 0.3 (see figure 2.3). In the present work the best measured power law dependences, shown in figure 5.8, are quite similar for submergence ratio equal to $0.5\,(h20)$, ranging from -0.34 (Veg1338) to -0.55 (Veg669) and slightly greater for a submergence ratio closer

to 0.3 ($h30$), ranging from -0.37 (Veg1338) to -0.58 (Veg251). It should be pointed out that data are quite scattered and confidence intervals of the prediction are wide.

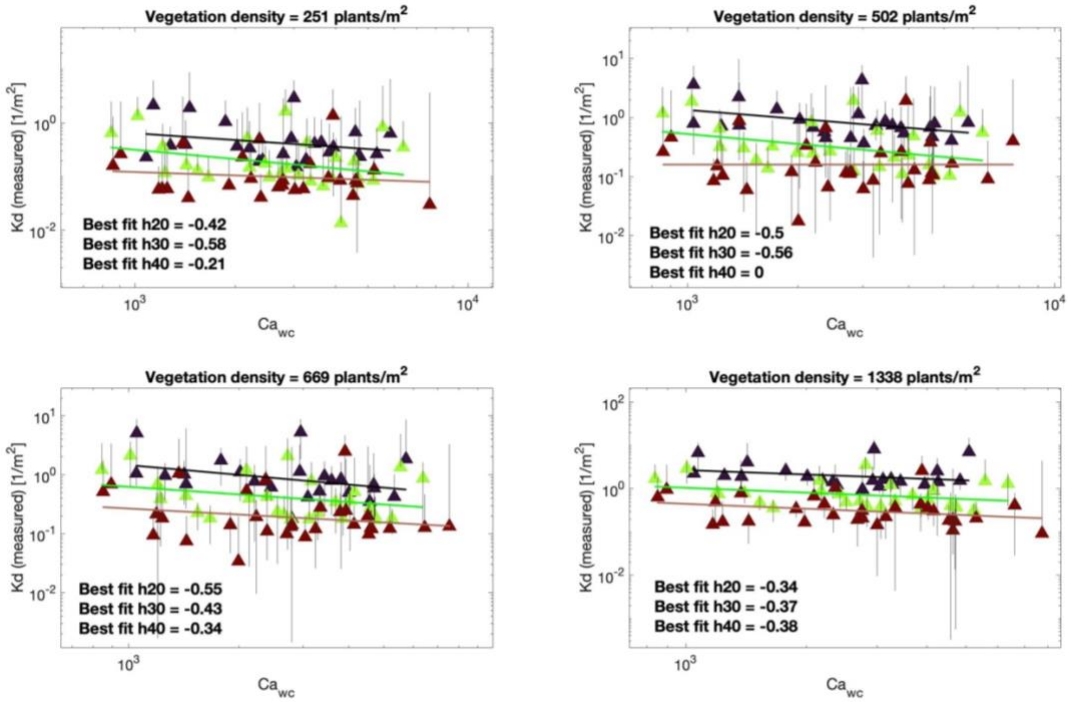

Figure 4.8: measured wave dissipation coefficient $K_{D,wc}$ for wave-current flows as a function of the wave-current Cauchy number Ca_{wc}. Solid black line denotes best linear fit for h20, solid green line denotes best linear fit for h30 and solid brown line denotes best linear fit for h40

The dissipation coefficient decreases with the wave-current Cauchy number as expected: Ca_{wc} depends directly on total in-canopy velocity, thus a greater velocity causes higher reconfiguration, deflecting blades and reducing wave energy dissipation. This is consistent with studies of wave attenuation in pure-wave conditions, for which $K_{D,pw}$ decreased with increasing wave Cauchy number Ca_w (Luhar et al., 2017), and in combined wave-current conditions, as mentioned above about Schaefer & Nepf (2022). Combining all the data the result is $K_{D,wc} \sim {Ca_{wc}}^{-0.36\pm0.23}$. Neglecting the 95% confidence interval, this result is consistent with the theoretical dependence assumed by equation (2.37), supporting the use of the effective meadow length $l_{e,m,wc}$ as predictor of the impact of reconfiguration in predicting wave attenuation. The theoretical power law is obtained by recalling $l_{e,m,wc} \sim {Ca_{wc}}^{-0.33}$ from equation (2.15) and approximating

$\sinh(kl_{e,m,wc}) \sim kl_{e,m,wc}$. The latter is valid only if $kl_{e,m,wc}$ is small, that is not the case in the present work, but for simplicity the influence of wave characteristics has been neglected.

From figure 5.8 it is evident that for shallower water depths, meaning higher submergence ratios, the wave attenuation is higher, reflecting that meadow are more effective in reducing wave amplitude when they occupy a larger fraction of water column, as observed also in pure-wave conditions by (Stratigaki et al., 2011; Manca et al., 2012; Luhar et al., 2017). It can be noticed that increasing vegetation density the dissipation coefficient increases, as expected from literature, because of the increased frontal area exposed to the flow that increase hydrodynamic drag. Moreover, increasing vegetation, data scattering decrease and confidence intervals on predictions become smaller.

Model proposed by Schaefer & Nepf (2022) implies that there should be a linear dependence between the dissipation coefficient and the drag coefficient of a plant in the flow of interest. Assuming that $C_{D,wc} \approx C_{D,pw}$, it follows $K_{D,wc} \sim KC^{-0.33}$, considering equation (2.3). An increase in Keulegan-Carpenter number is related with a decrease in drag coefficient and, in turn, with an increase in the dissipation coefficient.

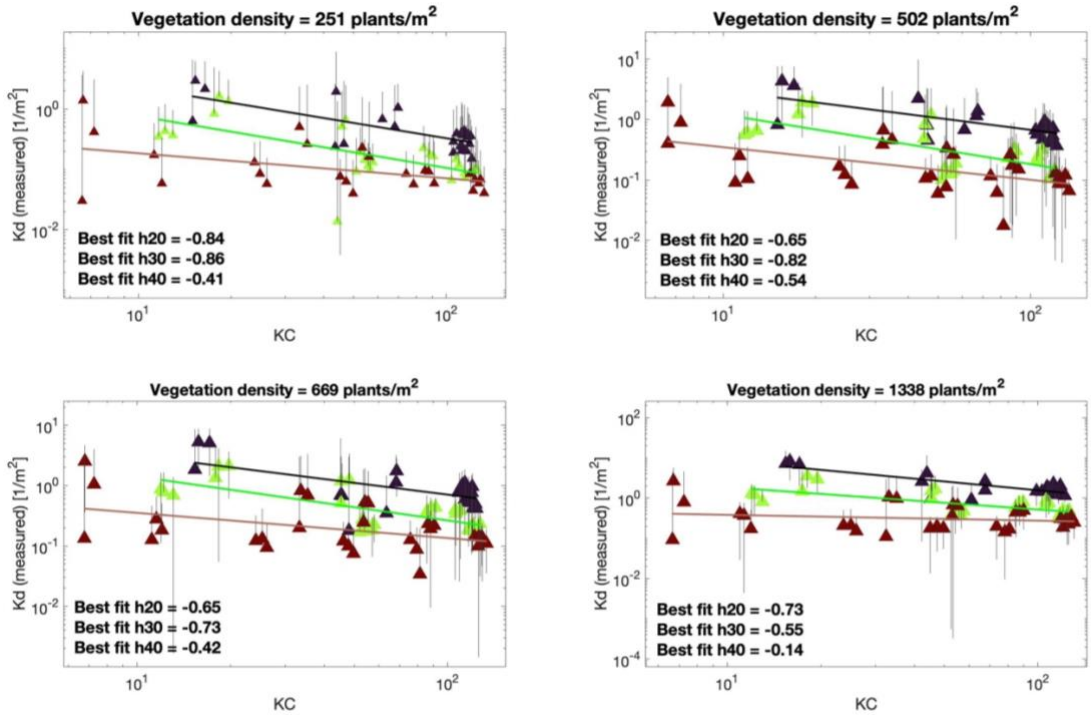

Figure 4.9: measured wave dissipation coefficient $K_{D,wc}$ for wave-current flows as a function of the Keulegan-Carpenter number KC. Solid black line denotes best linear fit for h20, solid green line denotes best linear fit for h30 and solid brown line denotes best linear fit for h40

Considering all the data the relationship obtained in the present work is $K_{D,wc} \sim KC^{-0.31\pm0.14}$. The mean value obtained is coherent with the theory abovementioned and confirms that the interaction between flow and a single plant in combined wave-current conditions can be modelled as in pure-wave conditions and that the dependence of $K_{D,wc}$ is very close to a linear one. However, it should be pointed out that individual datasets (e.g. one vegetation density at one water depth) have exponents that vary a bit. It appears that plant density and submergence ratio have some effect that is not completely captured by the model.

Both Losada et al. (2016) and Schaefer & Nepf (2022) models predict a linear dependence of dissipation coefficient on vegetation frontal area per unit meadow, the parameter related to meadow density. In particular, wave energy dissipation increases with increasing frontal area of the meadow.

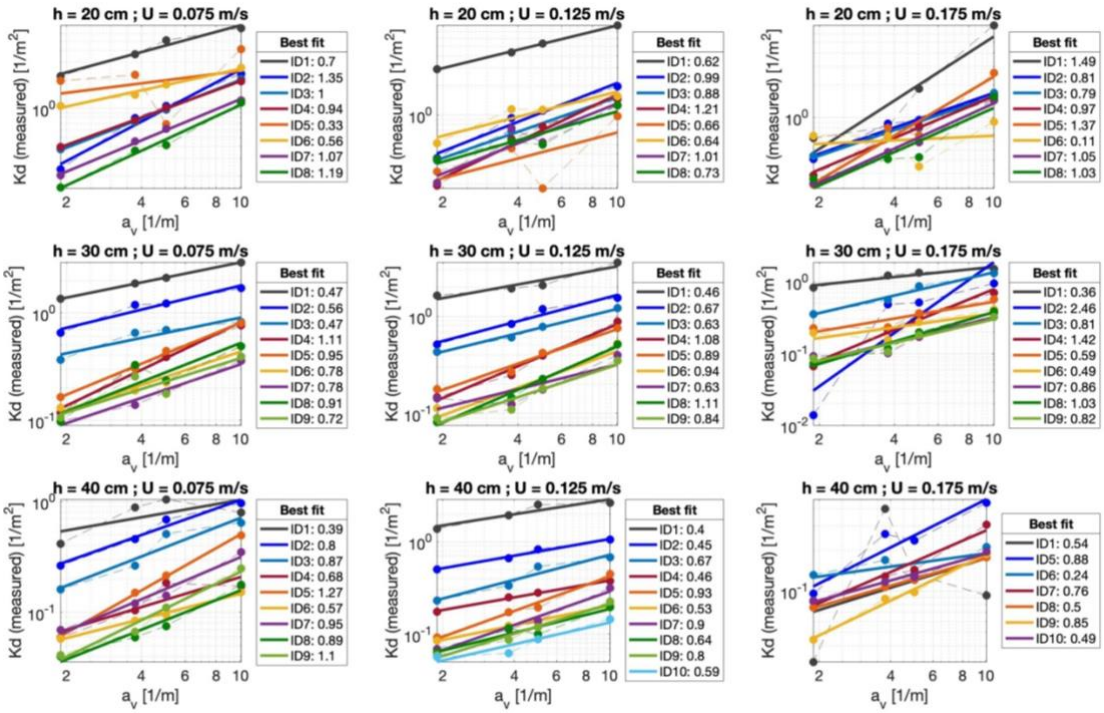

Figure 4.10: measured wave dissipation coefficient $K_{D,wc}$ for wave-current flows as a function of the vegetation frontal area per unit meadow a_v.

In the present work, combining all data, dissipation coefficient does not increase linearly with vegetation density. Specifically, $K_{D,wc} \sim {a_v}^{0.77\pm0.20}$. The increase in the number of plants reduces the velocity downstream each plant, due to wake effects. Drag of plants located in the wakes caused by upstream plants is lower and thus wave energy dissipation generated. By increasing vegetation densities, more plants ended up in wakes and so the wave dissipation increase is limited. Moreover, sheltering between blades can become significant increasing vegetation density and may not increase the frontal area that oppose resistance to the flow, limiting the increase in the dissipation of energy. These mechanisms are relevant in experiments in which the power fit between $K_{D,wc}$ and a_v is lower than one.

From figure 5.10 it is possible to observe that increasing water depth, or decreasing submergence ratio the dissipation coefficients increase less with vegetation density. The same behaviour, meaning less variation of $K_{D,wc}$ as function of wave-current Cauchy number Ca_{wc} and Keulegan-Carpenter number KC, can be observed respectively in figure 5.9 and figure 5.8. The lower is the submergence ratio, the less is the variation in wave dissipation caused by changes in the interaction

between flow and a single plant or between flow and meadows. Therefore, attenuation properties of meadows are more relevant when vegetation occupies a larger fraction of water depth , because the flow is more influenced by the presence of seagrass.

5. CONCLUSIONS AND FUTURE WORK

Seagrass contributes to reducing wave amplitude in both pure-wave and combined wave-current flows. Attenuation in wave height is due to the resistance that plants oppose to the flow, reducing its energy. Interaction between waves and a following current is strongly nonlinear, hence it is quite difficult to predict wave dissipation due to vegetation in those types of flows. The impact of a following current in dissipation mechanism can be observed in two main aspects: plant reconfiguration and hydrodynamic drag. Blades bend and deflect under the influence of a current and reduce the area that oppose resistance to the flow. Current contributes to increase total in-canopy velocity and dampen wave-induced motion, which, in turn, increase the hydrodynamic drag, due to the increase in relative velocity between flow and plants, that causes wave attenuation along the meadow.

In the literature two main models that predict wave dissipation in combined wave-current conditions exist: Losada et al. (2016) and Schaefer & Nepf (2022). They describe the interaction between waves and current as linear, assuming a uniform and irrotational wave-current field. They have been compared with experimental results obtained in this study and it has been observed that Schaefer & Nepf, 2022 model presents a good agreement, with the application of some corrections. This model makes use of the effective meadow length as parameter to describe the interaction between flow and canopy, incorporating in it all the blades bending and motion effects.

In the present study the addition of a following current contributes to reduce wave dissipation in almost all the cases. This result partially disagrees with Schaefer & Nepf (2022), who observed a negligible impact for currents with a time-averaged velocity equal half or less than the orbital wave velocity at canopy top, due to some differences in the characteristics of the tested waves, in particular of wave period.

Correlation between wave attenuation in combined wave-current conditions and dimensionless numbers that model the impact of a following current on the system (drag coefficient to model hydrodynamic drag and wave-current Cauchy number to model plant reconfiguration) is similar to what has been observed by Schaefer & Nepf (2022). On the other hand, the increase in wave attenuation related to the

increase in meadow density is not linear as observed and modelled in literature, due to sheltering and wake effects.

The present study can be considered as a starting point in the analysis of wave attenuation in combined wave-current flows. This topic should be studied focusing on the underlying physical process and considering the complexity of nonlinear interaction between current and waves. Further analysis should be performed on attenuation coefficients measured with the aim of identifying the most influent parameters on wave attenuation. Moreover, further analysis on the data collected can be performed, for example filtering the free surface level signals so that main harmonic could be isolated and become more similar to the theoretical linear waves.

BIBLIOGRAPHY

Baddour, R. E., & Song, S. (1990). On the interaction between waves and currents. *Ocean Engineering*, *17*(1–2), 1–21.

Belcher, S. E., Jerram, N., & Hunt, J. C. R. (2003). Adjustment of a turbulent boundary layer to a canopy of roughness elements. *Journal of Fluid Mechanics*, *488*, 369–398.

Beth Schaefer, R., & Nepf, H. (2022). Wave damping by seagrass meadows in combined wave-current conditions. *Limnology and Oceanography*.

Bradley, K., & Houser, C. (2009). Relative velocity of seagrass blades: Implications for wave attenuation in low-energy environments. *Journal of Geophysical Research: Earth Surface*, *114*(F1).

Chen, W. L., Muller, P., Grabowski, R. C., & Dodd, N. (2022). Green nourishment: an innovative nature-based solution for coastal erosion. *Frontiers in Marine Science*, *8*, 814589.

Citrini, D., & Noseda, G. (1987). Idraulica, Casa ed. *Ambrosiana, Milano, Seconda Ed*.

Dalrymple, R. A., Kirby, J. T., & Hwang, P. A. (1984). Wave diffraction due to areas of energy dissipation. *Journal of Waterway, Port, Coastal, and Ocean Engineering*, *110*(1), 67–79.

Davis, M., Krüger, I., & Hinzmann, M. (2015). Coastal Protection and Suds-Nature-Based Solutions. *RECREATE Project Policy Brief*, *4*.

de los Santos, C. B., Vicencio-Rammsy, B., Lepoint, G., Remy, F., Bouma, T. J., & Gobert, S. (2016). Ontogenic variation and effect of collection procedure on leaf biomechanical properties of Mediterranean seagrass Posidonia oceanica (L.) Delile. *Marine Ecology*, *37*(4), 750–759.

Dean, R. G., & Dalrymple, R. A. (1991). *Water wave mechanics for engineers and scientists* (Vol. 2). world scientific publishing company.

Folkard, A. M. (2005). Hydrodynamics of model Posidonia oceanica patches in shallow water. *Limnology and Oceanography*, *50*(5), 1592–1600.

Graham, J. M. R. (1980). The forces on sharp-edged cylinders in oscillatory flow at low Keulegan–Carpenter numbers. *Journal of Fluid Mechanics*, *97*(2), 331–346.

Hu, Z., Suzuki, T., Zitman, T., Uittewaal, W., & Stive, M. (2014). Laboratory study on wave dissipation by vegetation in combined current–wave flow. *Coastal Engineering*, *88*, 131–142.

Infantes, E., Orfila, A., Simarro, G., Terrados, J., Luhar, M., & Nepf, H. (2012). Effect of a seagrass (Posidonia oceanica) meadow on wave propagation. *Marine Ecology Progress Series*, *456*, 63–72.

Keulegan, G. H., & Carpenter, L. H. (1958). Forces on cylinders and plates in an oscillating fluid. *Journal of Research of the National Bureau of Standards*, *60*(5), 423–440.

Lei, J., & Nepf, H. (2019a). Blade dynamics in combined waves and current. *Journal of Fluids and Structures*, *87*, 137–149.

Lei, J., & Nepf, H. (2019b). Wave damping by flexible vegetation: Connecting individual blade dynamics to the meadow scale. *Coastal Engineering*, *147*, 138–148.

LeMéhauté, B. (1969). *An introduction to hydrodynamics and water waves* (Vol. 52). Environmental Science Servies Administration.

Li, C. W., & Yan, K. (2007). Numerical investigation of wave–current–vegetation interaction. *Journal of Hydraulic Engineering*, *133*(7), 794–803.

Losada, I. J., Maza, M., & Lara, J. L. (2016). A new formulation for vegetation-induced damping under combined waves and currents. *Coastal Engineering*, *107*, 1–13.

Lowe, R. J., Koseff, J. R., & Monismith, S. G. (2005). Oscillatory flow through submerged canopies: 1. Velocity structure. *Journal of Geophysical Research: Oceans*, *110*(C10).

Luhar, M., Infantes, E., & Nepf, H. (2017a). Seagrass blade motion under waves and its impact on wave decay. *Journal of Geophysical Research: Oceans*, *122*(5), 3736–3752.

Luhar, M., Infantes, E., & Nepf, H. M. (2017b). Seagrass blade motion under waves and its impact on wave decay. *Journal of Geophysical Research: Oceans*, *122*, 3736–3752. https://doi.org/10.1002/2017JC012731

Luhar, M., & Nepf, H. M. (2016). Wave-induced dynamics of flexible blades. *Journal of Fluids and Structures*, *61*, 20–41.

Manca, E., Cáceres, I., Alsina, J. M., Stratigaki, V., Townend, I., & Amos, C. L. (2012). Wave energy and wave-induced flow reduction by full-scale model Posidonia oceanica seagrass. *Continental Shelf Research*, *50*, 100–116.

Mendez, F. J., & Losada, I. J. (2004). An empirical model to estimate the propagation of random breaking and nonbreaking waves over vegetation fields. *Coastal Engineering*, *51*(2), 103–118.

Ondiviela, B., Losada, I. J., Lara, J. L., Maza, M., Galván, C., Bouma, T. J., & van Belzen, J. (2014). The role of seagrasses in coastal protection in a changing climate. *Coastal Engineering*, *87*, 158–168.

Paul, M., Bouma, T. J., & Amos, C. L. (2012). Wave attenuation by submerged vegetation: combining the effect of organism traits and tidal current. *Marine Ecology Progress Series*, *444*, 31–41.

Sarpkaya, T., & Storm, M. (1985). In-line force on a cylinder translating in oscillatory flow. *Applied Ocean Research*, *7*(4), 188–196.

Seddon, N., Chausson, A., Berry, P., Girardin, C. A. J., Smith, A., & Turner, B. (2020). Understanding the value and limits of nature-based solutions to climate change and other global challenges. *Philosophical Transactions of the Royal Society B*, *375*(1794), 20190120.

Soissons, L. M., van Katwijk, M. M., Peralta, G., Brun, F. G., Cardoso, P. G., Grilo, T. F., Ondiviela, B., Recio, M., Valle, M., & Garmendia, J. M. (2018). Seasonal and latitudinal variation in seagrass mechanical traits across Europe: the influence of local nutrient status and morphometric plasticity. *Limnology and Oceanography*, *63*(1), 37–46.

Stratigaki, V., Manca, E., Prinos, P., Losada, I. J., Lara, J. L., Sclavo, M., Amos, C. L., Cáceres, I., & Sánchez-Arcilla, A. (2011). Large-scale experiments on wave propagation over Posidonia oceanica. *Journal of Hydraulic Research*, *49*(sup1), 31–43.

Taylor, J. R. (1997). An introduction to error analysis, 327 pp. *Univ. Sci. Books, Sausalito, Calif.*

Vettori, D., & Marjoribanks, T. I. (2021). Temporal variability and within-plant heterogeneity in blade biomechanics regulate flow-seagrass interactions of Zostera marina. *Water Resources Research*, *57*(3), e2020WR027747.

Yin, Z., Wang, Y., Liu, Y., & Zou, W. (2020). Wave attenuation by rigid emergent vegetation under combined wave and current flows. *Ocean Engineering*, *213*, 107632.

Zhang, X., & Nepf, H. (2021). Wave damping by flexible marsh plants influenced by current. *Physical Review Fluids*, *6*(10), 100502.

Zhao, C., Tang, J., Shen, Y., & Wang, Y. (2021). Study on wave attenuation in following and opposing currents due to rigid vegetation. *Ocean Engineering*, *236*, 109574.